RESEARCH REPORT

NO VTT-R-01025-09| 15.4.2009

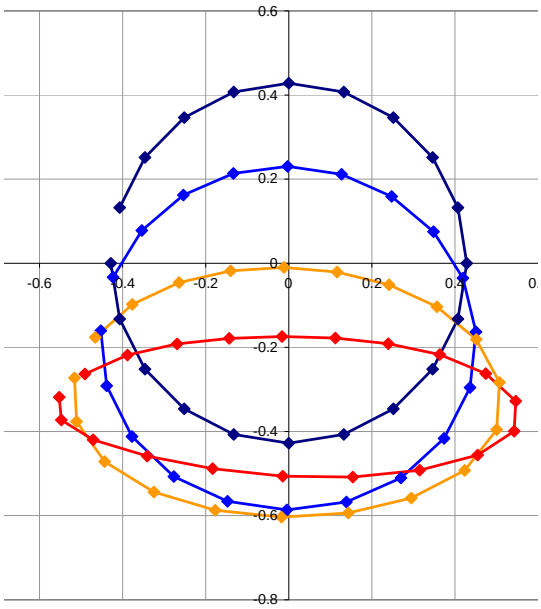

SAFIR 2010 FRAS

Numerical Studies on Dynamic Behaviour of Pipelines

Authors: Kim Calonius

Confidentiality: Public

Report's title Numerical Studies on Dynamic Behaviour of Pipelines	
Customer, contact person, address SAFIR 2010 VYR	Order reference
Project name **Fracture assessment for reactor circuit (**FRAS) / Loads transferred by supports	Project number/Short name 13511-FRAS
Author(s) Kim Calonius	Pages 50/
Keywords **loads supports pipe break FEM reactor circuit**	Report identification code VTT-R-01025-09

Summary

Dynamic excitation due to a pipe break can cause pipe to abruptly displace and hit the components, instrumentation and equipment nearby. In order to minimize the extensive damage caused by such pipe whips, different types of restraints and supports are designed for the pipelines.

Here, structural dynamic behaviour of pipelines is studied with finite element method. A relatively short pipe line section with one bend and one restraint and rigidly fixed from its other end is chosen as a test case. The usability of different types of elements provided by Abaqus code (mainly version 6.7) in modelling the pipe, restraint and adjacent civil structure is tested.

First, the stiffness of the restraint as well as the flexural stiffness of the pipe cross-section are solved with static analyses with a detailed model using three-dimensional solid and shell elements. After that, the model is substituted with couple of simpler models using pipe or elbow and special-purpose elements such as pipe, elbow, spring and pipe support elements having the corresponding stiffness properties.

The eigenmodes of models are calculated and compared with each other. The pipe whip is simulated with nonlinear dynamic analyses. The displacement and stress results of different models are compared with each other and the reliability and adequacy of different element types are discussed. Sensitivity study is made by varying the analysis type, material properties, mesh density and element properties (interpolation, number of integration points and ovalization modes).

The results of the most adequate simple models with the right combinations of elbow and special-purpose elements provided by Abaqus corresponded well to the ones of the much larger three-dimensional solid and shell element models. Long pipe runs should preferably be modelled with pipe, elbow and special-purpose elements in order to save time and prevent errors due to overly large and complicated models.

Confidentiality	Public

Espoo 15.4.2009

Signatures	Signatures	Signatures
Written by Kim Calonius, Research Scientist	Reviewed by Arja Saarenheimo, Senior Research Scientist	Accepted by Eila Lehmus, Technology Manager

VTT's contact address
P.O.Box 1000, 02044 VTT

Distribution (customer and VTT)
SAFIR2010 Reference Group 6
SAFIR2010 FRAS Ad Hoc Group

Preface

This report has been prepared under the research project FRAS 1.1; “Loads Transferred by Supports”, which concerns external loads transferred to the reactor circuit components by different types of supports. The project is a part of SAFIR2010, which is a national nuclear energy research program. FRAS 1.1 project work in 2008 was funded by the State Nuclear Waste Management Fund (VYR) and the Technical Research Centre of Finland (VTT). The work was carried out at VTT. The author of the report expresses his gratitude to Arja Saarenheimo (VTT) for her valuable expertise and help and to Pekka Nevasmaa (VTT) and Päivi Karjalainen-Roikonen (VTT) for managing FRAS project.

Espoo 15.4.2009

Author

Contents

1 Introduction

This report is a deliverable for the first year of the project called “Loads transferred by supports” funded by VYR and VTT. It is a sub-project of a larger project called FRAS (Fracture Assessment for Reactor Circuit**)** which for its part belongs to a national multidisciplinary SAFIR2010 research programme on nuclear power plant safety for the years 2007-2010. SAFIR2010 is strongly based on the chapter 7a, “Ensuring expertise”, of the Finnish Nuclear Energy Act. The programme is the newest link in chain of public research programmes on nuclear safety that maintain and develop the respective know-how in Finland.

The greatest uncertainties in the assessment of structural integrity of a component are generally associated with the accurate determination of loads. This subproject “Loads transferred by supports” aims at calculating of both design and unforeseeable loads and their effects on a structure by applying numerical modelling.

The main objective is to define the external loads transferred to the reactor circuit components by supports. The study will concentrate on certain components and simulate their behaviour under some unforeseeable, critical accident loads numerically with finite element method. During the first year, modelling methods for different types of supports and restraints were delineated. Stiffnesses of pipes and its supports were calculated with finite element method and substituted with simpler structural and special-purpose elements. A pipe break was chosen as a test case that was simulated with different kinds of models. The results were compared with each other and their reliabilities were evaluated. More of the first year’s study can be found in VTT public research report (Calonius, 2008).

In this report, the same short section of a pipeline is studied in more detail. More element types are compared by means of eigenfrequency extraction. Also nonlinear material properties are included.

The results can be applied to assess structural safety of nuclear reactor components, as well as to evaluate their remaining lifetime during service, by coupling between advanced numerical modelling tools and material’s characterisation data, in order to cover the entire chain of structural safety related aspects coupling the interaction of effects of loads, existing flaws, material’s relevant damage mechanims and degradation of properties during service.

2 Finite element modelling of pipelines

Every continuum structure can be modelled and solved with general-purpose solid continuum volume elements. However, that can be very ineffective and time-consuming, since usually very large amount of volume elements are needed to catch the right behaviour. That is why it is useful to have structural and special-purpose elements instead.

The pipes in power plants are long, slender structures with relatively thin walls. That is why it is convenient to model them with shell elements. Since the beam theory can be used to calculate their behaviour quite accurately, also pipe elements can be used. Beam, elbow, shell and solid volume elements are used in this study for modelling the pipe. In the future, also so called continuum shell elements are worth trying.

There are many types of supports and restraints in power plants. They support components and pipelines mainly against the gravitational forces in vertical direction. Either the components rest on the support or they are suspended by the so-called hangers. The function of restraints is to take the dynamic loads in case of accidents such as pipe breaks or earthquakes when the pipes can have exceptionally large movements and velocities. The thermal expansion is taken into account by leaving sufficiently large gaps between the pipe and restraints.

If special-purpose elements are not used, contact behaviour has to be formulated between the pipe and restraint surfaces. That is why it is also useful to have special-purpose elements instead, which can include the gap, contact, stiffness and even possible viscous properties. Those elements in Abaqus (Abaqus, 2007) include for instance:

- Spring elements
- Dashpot elements
- Tube support elements
- Gap elements
- Tube-to-tube elements
- Frame elements
- Connector elements

Solid volume and nonlinear spring elements are used in this study for modelling the restraint.

3 Model description

Since all kinds of sensitivity study is made and adequacy of different model types is assessed, it is practical that the structure is not too complex with many variables. A relatively short pipe section with one restraint and one bend is studied. The whole combined model consists of three parts: the pipe, the restraint with a small gap (approximately 6 cm), and a concrete block which represents the civil works or containment wall near the pipeline. Figure 2 shows the example pipeline geometry simulated in this study with main dimensions. In the following analyses, the lower right end of the pipe is rigidly fixed, unless otherwise mentioned. The postulated pipe break takes place in the upper left end of the section.

The different finite element model types are shown in Figure 3. The concrete block and the restraint are modelled either with solid volume elements (C3D8R) or with a nonlinear spring element (SPRINGA). The pipe is modelled with solid volume, shell, pipe or elbow elements. The detail of the solid volume element model of the pipe is shown in the upper left hand corner. It has four linear 8-noded elements through the wall thickness and altogether 272 136 elements (C3D8R). The pipe (or elbow) element model is shown in the upper right hand corner. Depending on the mesh density, it has either 18 or 36 elements (6 or 12 elements along the bend) (PIPE31, PIPE32, ELBOW31, ELBOW31B, ELBOW31C or ELBOW32). There are three different cases element wise: 1) only pipe elements are used, 2) only elbow elements are used or 3) pipe elements are used for the straight sections and elbow elements for the bend section. The spring element can also be seen near the bend in the horizontal section. The shell element model with a fine mesh is shown below the other two models. It has 44 shell elements (S4R) around the pipe circumference and the total number of elements is 6864. The model with a coarse mesh has only 12 elements around the pipe (total number of elements 456). In all the shell element models in this study, there are 5 integration points through the thickness of the wall.

Two materials are used, steel and concrete. The same steel is used both for the pipe and for the simple restraint with a square cross-section. Water is not included and its mass is not taken into account, but the high inner pressure is applied in some cases. Table 1 shows the material property values. The material properties for the linear elastic materials needed for the analyses are the density, the Young's modulus and the Poisson coefficient. In some cases also plastic properties are included by giving the stress strain curve as data pairs. The yield point (at 0.2 % plastic deformation in Mises yield surface) is 210 MPa. Properties in room temperature are used. Most probably again in the case of an accident, the material would be in operational temperature and thus have a lower yield point value. No rate dependency is defined. Figure 1 shows the logarithmic strain components as a function of true stress (stress being in y-axis as normally in stress-strain curves). In the constitutive model used, the elastic and plastic responses are totally distinguished into separate parts. The material is nearly linear elastic - ideal plastic material. In practical structures, it means that after exceeding the plastic limit load, a local plastic hinge develops very quickly and the structure loses its carrying capacity.

Table 1. Material properties.

material	steel	concrete
Density, ρ	7850 kg/m^3	2400 kg/m^3
Young's modulus, E	210 GPa	35 GPa
Poisson coefficient, ν	0.3	0.2
Yield point, σ	210 MPa	-

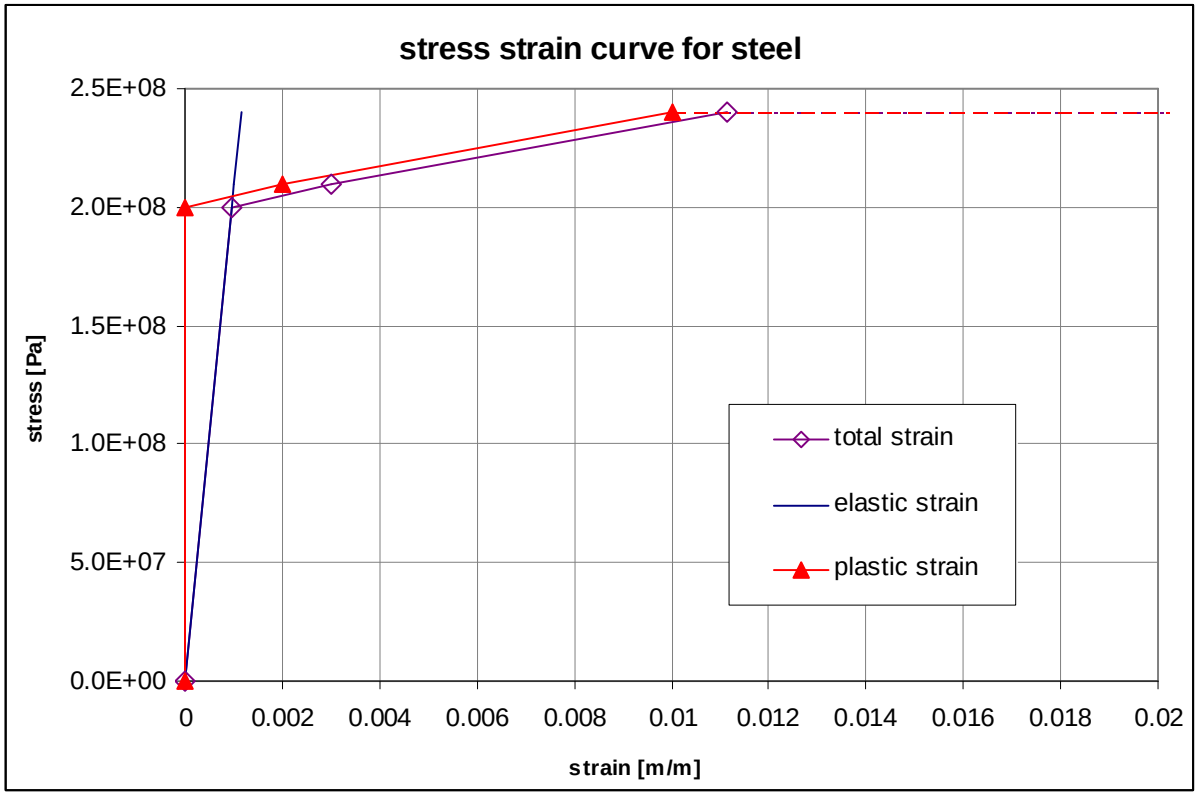

Figure 1. Stress strain curves (elastic, plastic and total strain) for steel.

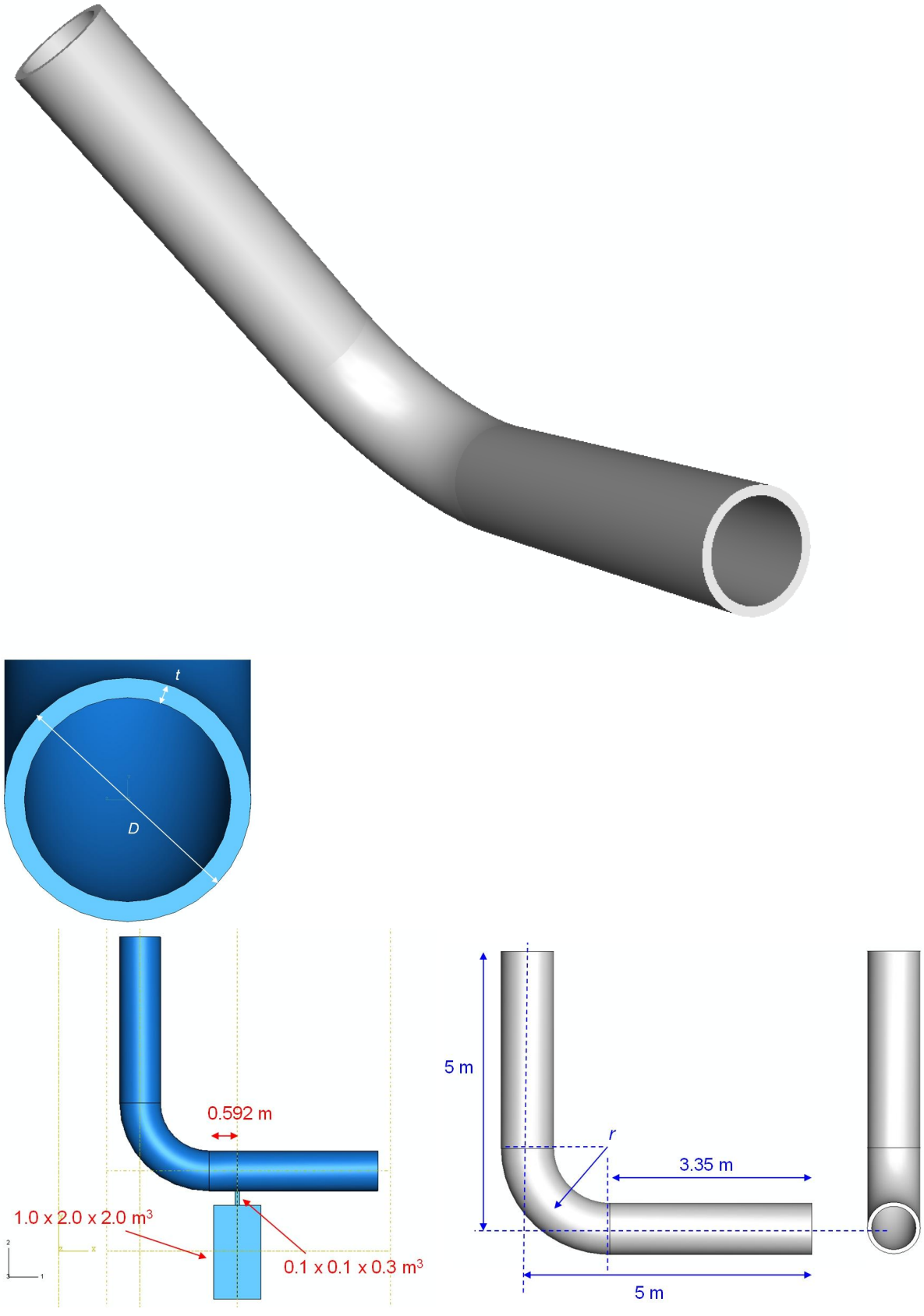

Figure 2. Example pipeline section with main dimensions.

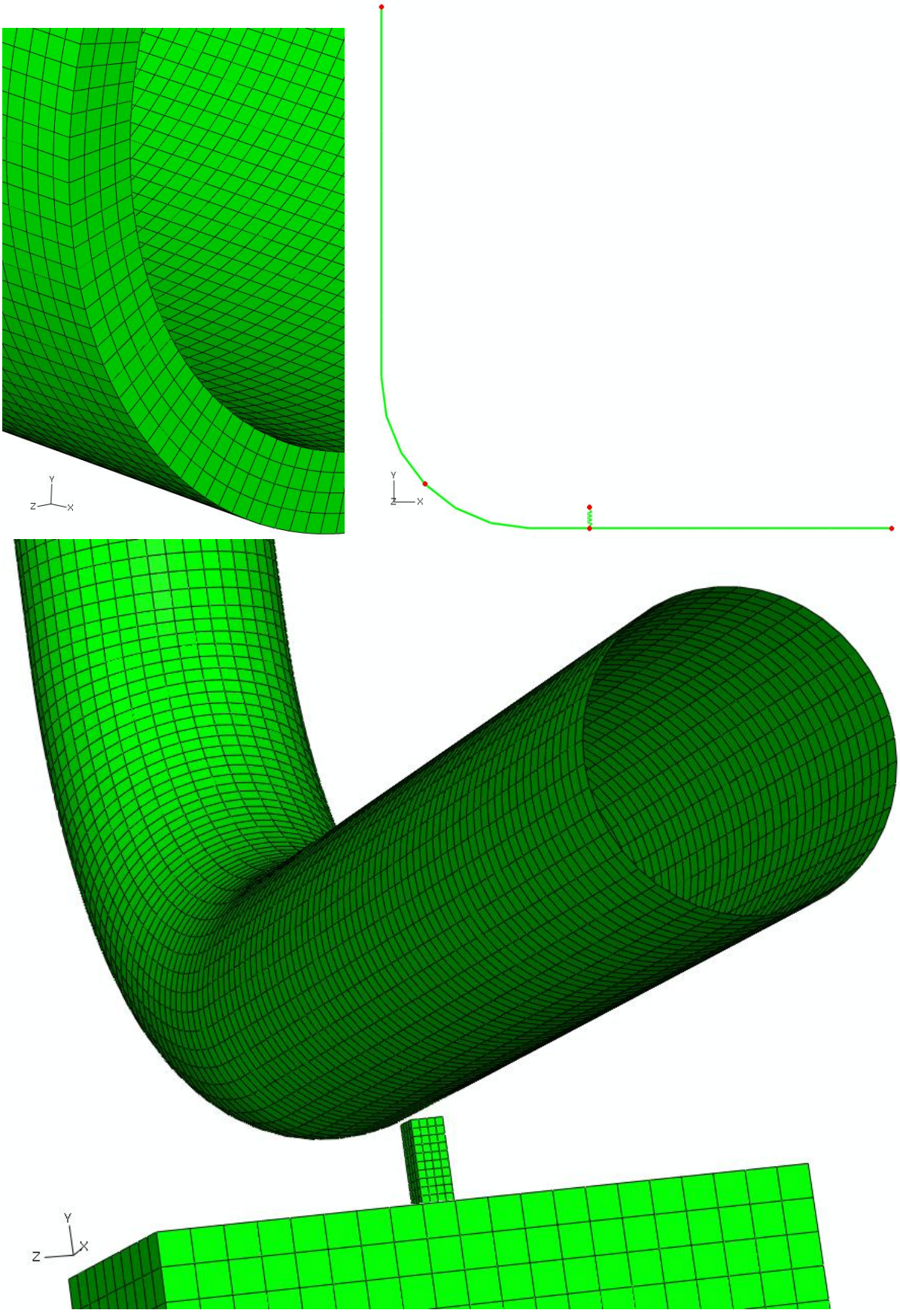

Figure 3. Solid volume, pipe and shell element models.

Figure 4 shows the pipe (or elbow) element model with node and element numbers. It has altogether 18 elements, horizontally 6, vertically 6 and also 6 elements modelling the pipe bend. Some analyses are conducted with a finer mesh, which has twice the amount of elements.

A previous study by Haapaniemi suggested that the use of more elbow elements (ELBOW31 in Abaqus code) than two in order to model a pipe bend is advisable especially with more complex structures and/or higher modes. Also, the results indicate that the benefits obtained if more than six elbow elements are being used in the bend are not necessarily very significant (Haapaniemi, 2002). Thus, it is expected, that for this study, six ELBOW31 elements capture the dynamic behaviour of the bend almost as accurately as pipe elements can.

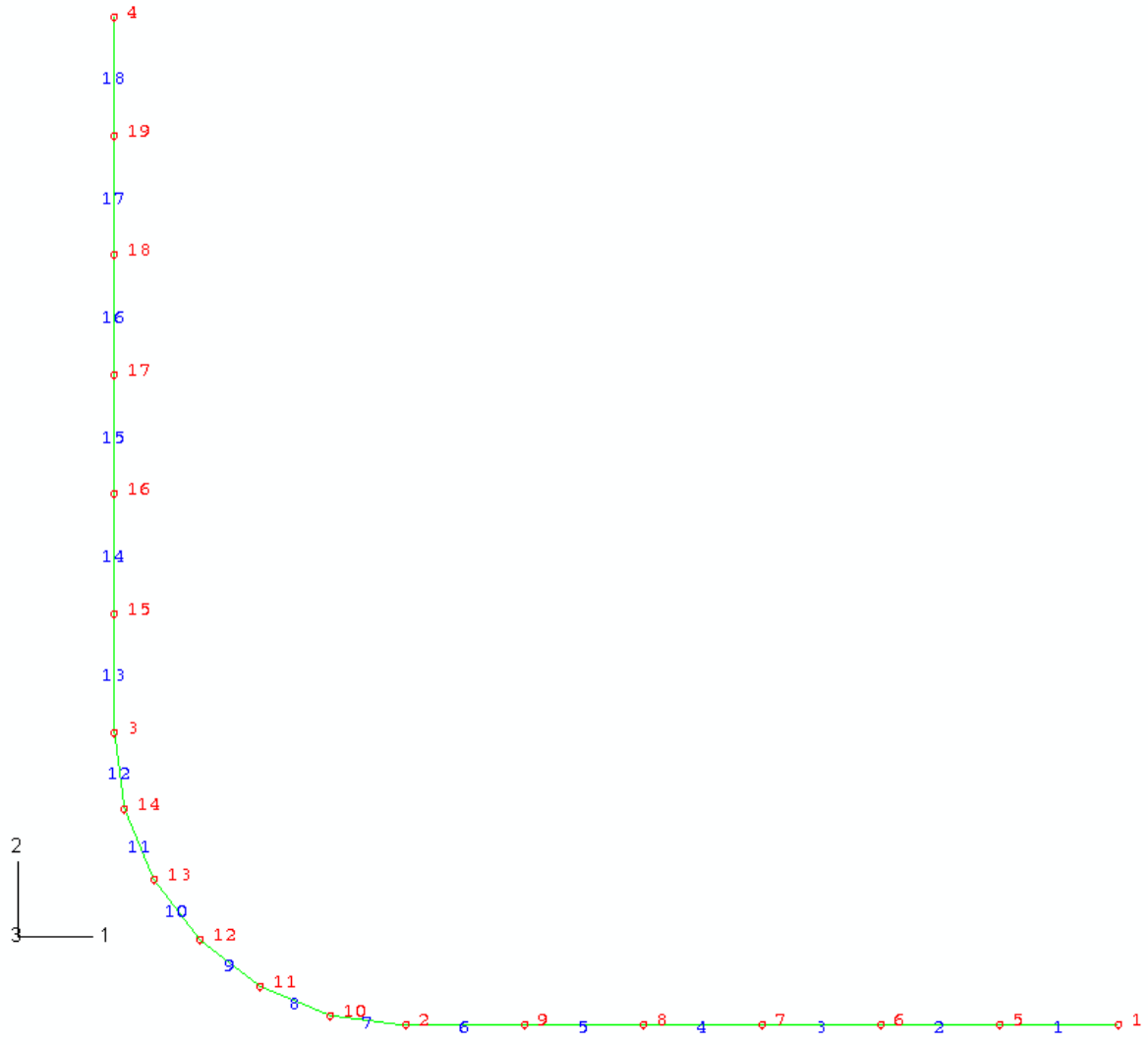

Figure 4. Pipe (or elbow) element model with node and element numbers.

4 Natural frequency extraction of a pipeline section

In order to find out the adequacy of different element types and the sensitivity of the models to different parameters many different cases are studied by extracting their natural frequencies and comparing them with each other. The models have to be linear, of course. There is no restraint. The lower end of the pipe is fixed and the upper end is free.

Altogether 19 different cases were solved. Following characteristics were varied: Element type and interpolation, mesh density, number of integration points and ovalization modes, whether the rotations are free in the fixed end of the shell element model, the inner pressure type with elbow elements (open or closed) and the inner pressure with shell elements. First ten eigenfrequencies were solved with Lanczos method and they are shown together with total mass of the model in Table 2. The heading tells the element type that is used. The last row tells the mean value of the absolute percentual difference between the corresponding eigenfrequencies of the 3D solid volume model (C3D8R, the first result row) and the compared model in question.

The default parameter values for elbow elements are used unless otherwise mentioned. There are five integration points through the pipe wall thickness and twenty around the pipe. The maximum available six Fourier ovalization modes are used. Element types ELBOW31B and ELBOW31C use a simplified version of the formulation, in which ovalization only is considered (no warping) and axial gradients of the ovalization are neglected. Also quadratic interpolation (instead of linear) along the pipe is used in some cases (for example PIPE32).

Table 2. Natural frequencies of different models.

	C3D8R	S4R shell fine mesh	S4R shell fine mesh rotation free	S4R shell fine mesh pressure	S4R shell coarse mesh	PIPE31	ELBOW31
mass (kg)	*15 040*	*15 032*	*15 032*	*15 032*	*14 862*	*15 035*	*15 045*
mode 1 (Hz)	10.847	10.834	10.821	11.223	10.585	11.311	10.839
mode 2 (Hz)	11.147	11.131	11.116	11.559	10.925	12.018	11.143
mode 3 (Hz)	28.181	28.202	28.136	28.580	28.139	33.330	28.226
mode 4 (Hz)	32.314	32.250	32.181	32.535	31.517	34.089	32.690
mode 5 (Hz)	105.86	106.03	105.78	106.38	105.93	115.35	118.99
mode 6 (Hz)	127.24	127.01	126.75	127.40	125.29	127.87	124.92
mode 7 (Hz)	150.85	151.11	151.00	151.56	150.69	160.35	181.86
mode 8 (Hz)	186.55	186.46	185.76	186.41	185.85	189.28	186.44
mode 9 (Hz)	215.11	214.90	214.11	214.97	213.02	216.63	220.52
mode 10 (Hz)	258.43	258.53	258.31	258.81	258.28	261.36	252.34
difference (%)		*0.12*	*0.26*	*1.06*	*1.01*	*5.49*	*4.11*

	PIPE31 + ELBOW31	PIPE31 + ELBOW31 fine mesh	ELBOW31 fine mesh	PIPE32 fine mesh	ELBOW32 fine mesh
mass (kg)	*15 045*	*15 045*	*15 045*	*15 045*	*15 045*
mode 1 (Hz)	10.674	10.696	10.854	11.320	10.858
mode 2 (Hz)	10.877	10.902	11.165	12.036	11.172
mode 3 (Hz)	27.086	27.107	28.160	33.565	28.138
mode 4 (Hz)	32.058	32.247	32.831	34.135	32.878
mode 5 (Hz)	102.95	103.17	118.72	115.59	118.63
mode 6 (Hz)	119.94	120.41	124.92	128.94	124.92
mode 7 (Hz)	149.63	150.16	182.53	161.45	182.75
mode 8 (Hz)	184.83	185.36	185.61	189.89	185.34
mode 9 (Hz)	214.21	216.36	220.92	218.99	221.06
mode 10 (Hz)	251.76	254.04	254.23	264.75	254.86
difference (%)	*2.19*	*1.89*	*4.17*	*6.07*	*4.21*

	ELBOW31B	ELBOW31C	ELBOW31 3 ovalization modes	ELBOW32 fine mesh pressure open	ELBOW32 fine mesh pressure closed
mass (kg)	*15 045*	*15 045*	*15 045*	*15 045*	*15 045*
mode 1 (Hz)	10.745	10.760	10.842	11.001	10.880
mode 2 (Hz)	10.939	10.962	11.147	11.192	11.200
mode 3 (Hz)	27.371	27.472	28.245	28.425	28.269
mode 4 (Hz)	32.235	32.265	32.694	32.613	32.933
mode 5 (Hz)	112.22	112.50	119.02	118.81	118.88
mode 6 (Hz)	116.67	116.94	124.94	125.67	125.12
mode 7 (Hz)	178.84	179.30	181.95	183.10	183.37
mode 8 (Hz)	183.35	183.52	186.47	184.16	185.58
mode 9 (Hz)	214.71	215.09	220.58	221.37	221.54
mode 10 (Hz)	249.92	250.10	252.36	255.32	255.08
difference (%)	*4.40*	*4.32*	*4.12*	*4.39*	*4.33*

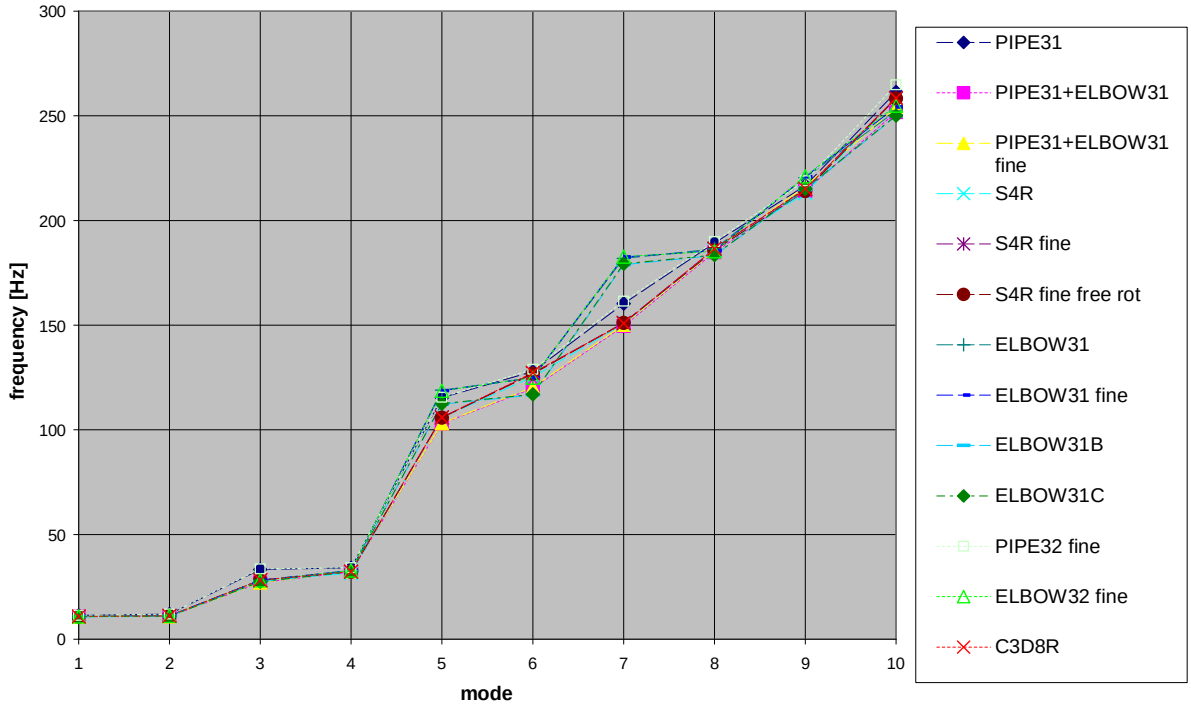

Figure 5. The eigenfrequencies [Hz] of different models.

The masses are really close to each other in every case, which partly verifies the models. The most accurate model can be assumed to be the one with solid volume elements (the first result column in Table 2) or perhaps the one with a very fine shell element mesh (the second column in Table 2). Their eigenfrequencies are very similar. The model with only linear pipe elements (the 6th column) has some discrepancies and is not accurate enough. The ones with also elbow elements correspond better with the detailed models. Only the 7th mode has got some major discrepancies (elbow element models being clearly stiffer). Figure 5 shows the eigenfrequencies of most of the models in a single chart. They are all relatively close to each other.

The deformed shapes of the first 10 modes of different model types (from left to right; PIPE31, C3D8R and S4R fine mesh) are shown in the next 10 figures (from Figure 6 to Figure 15). The second mode is the dominant mode in the pipe break case studied below. The mode 2 frequencies are coloured red in Table 2.

Whether the rotational degrees of freedom of the shell element model end are fixed or left free, does not make much difference. The inner pressure makes the models slightly stiffer. The model that used both pipe and elbow elements is really close to that when it comes to eigenfrequencies, even closer than the coarse shell model. Mesh refinement only very slightly enhances its accuracy in a global sense. However, in a local sense a fine mesh would give more detailed stress results. Two model types are chosen for the dynamic analyses: the model with a fine shell element mesh (the 2nd column) and the model with 18 linear elbow elements (the 7th column).

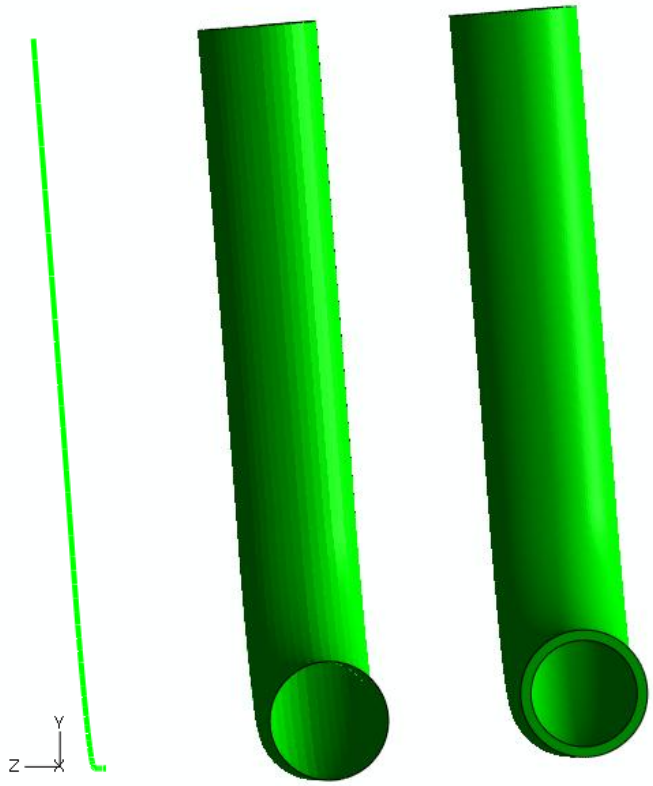

Figure 6. Mode 1 of different model types.

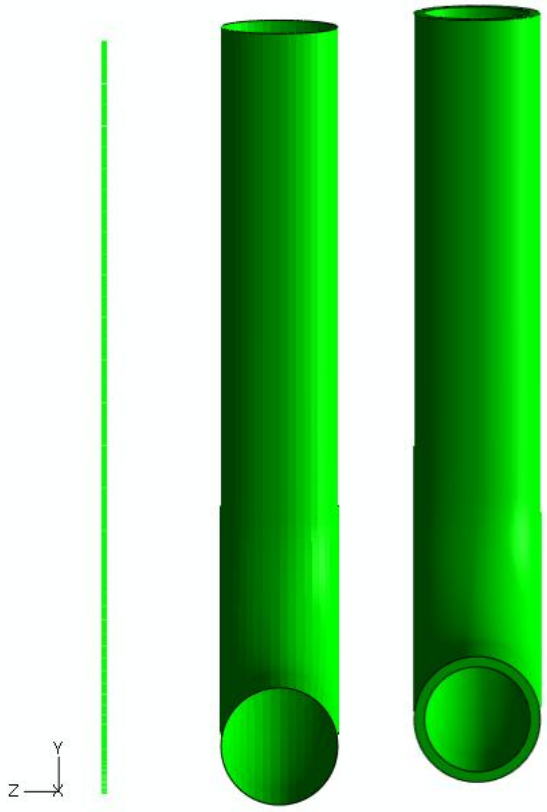

Figure 7. Mode 2 of different model types.

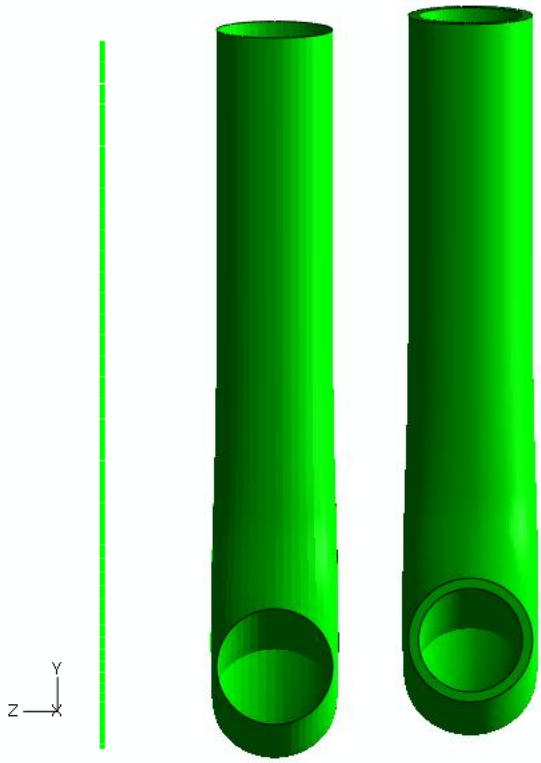

Figure 8. Mode 3 of different model types.

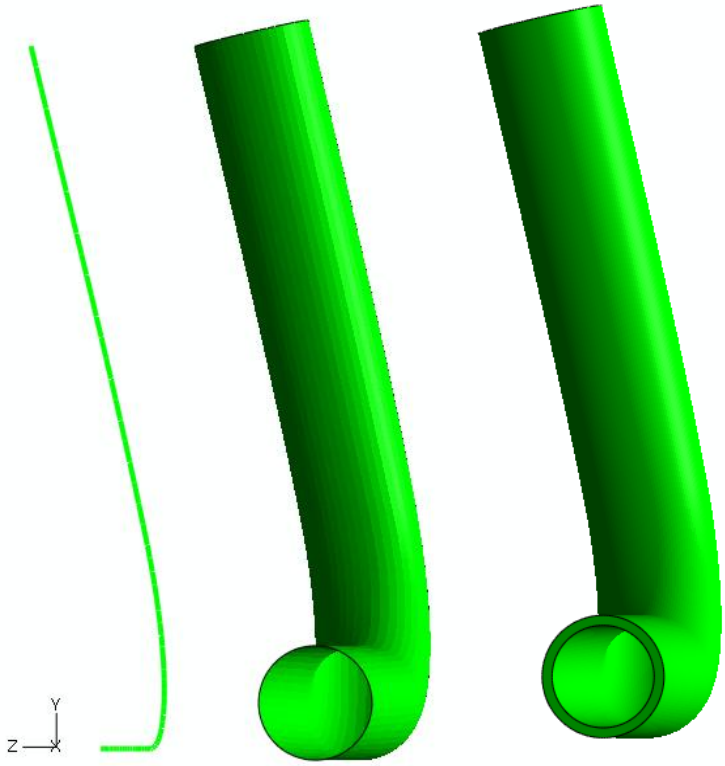

Figure 9. Mode 4 of different model types.

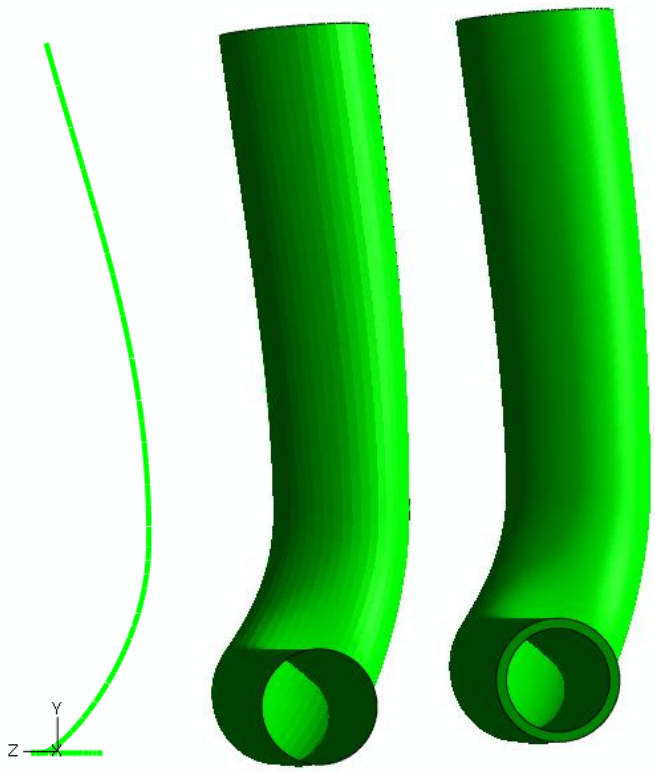

Figure 10. Mode 5 of different model types.

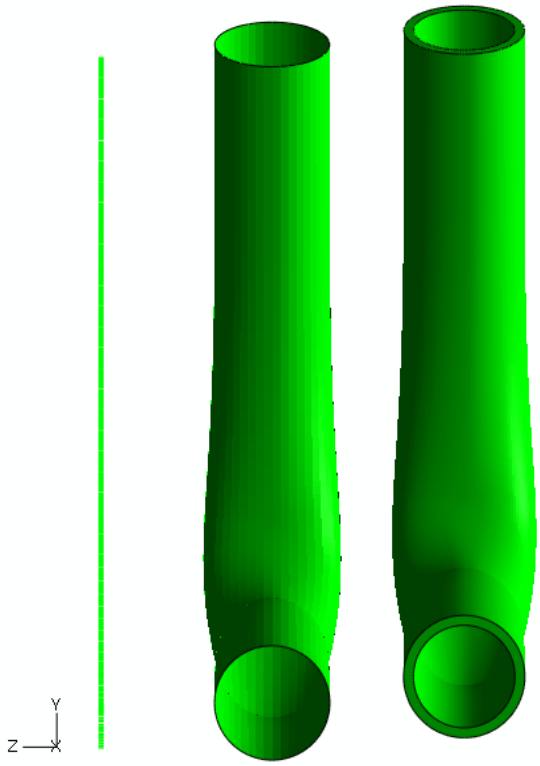

Figure 11. Mode 6 of different model types.

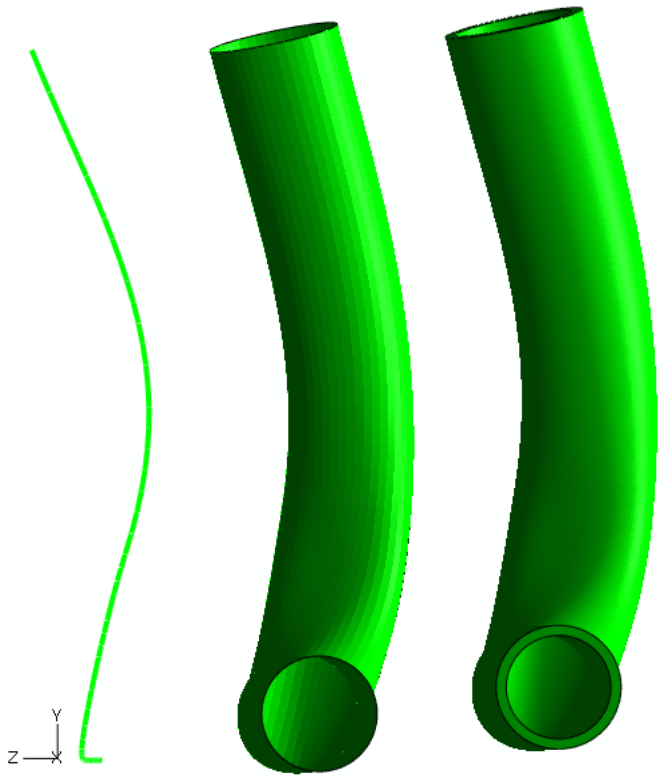

Figure 12. Mode 7 of different model types.

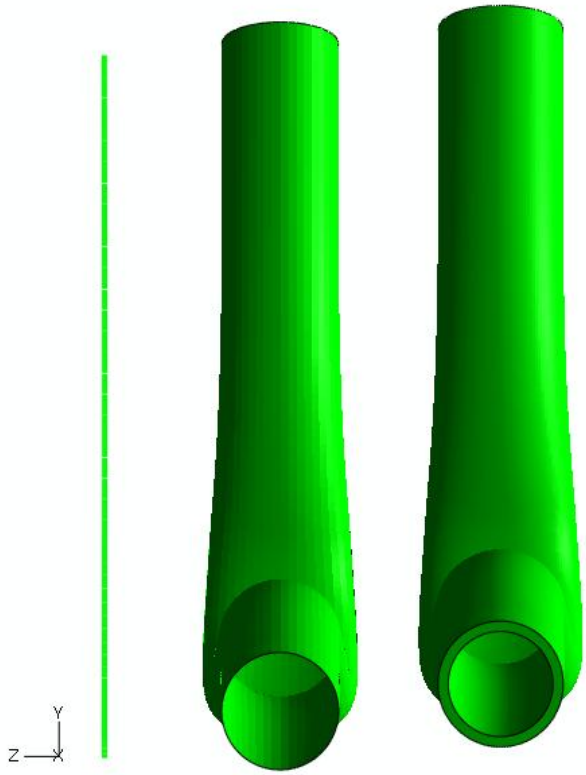

Figure 13. Mode 8 of different model types.

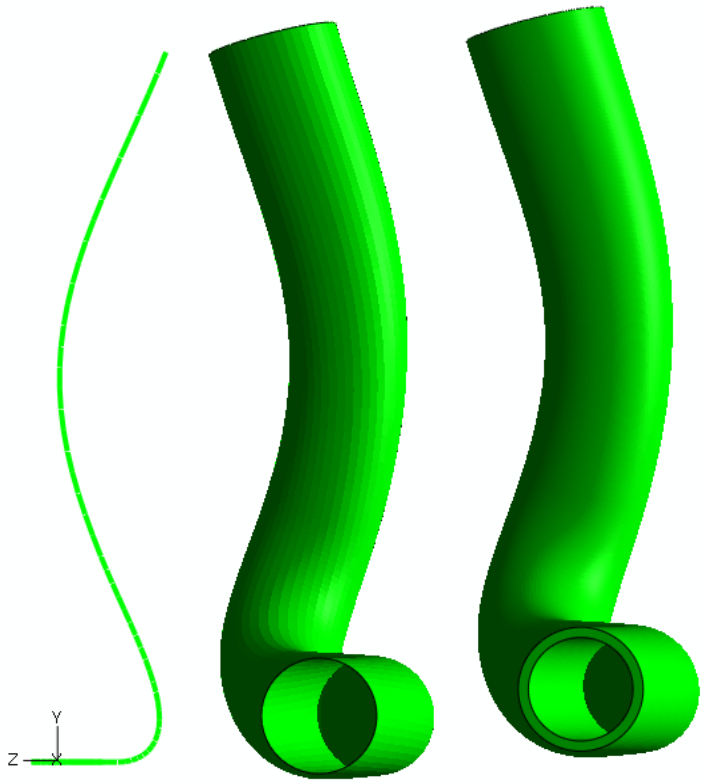

Figure 14. Mode 9 of different model types.

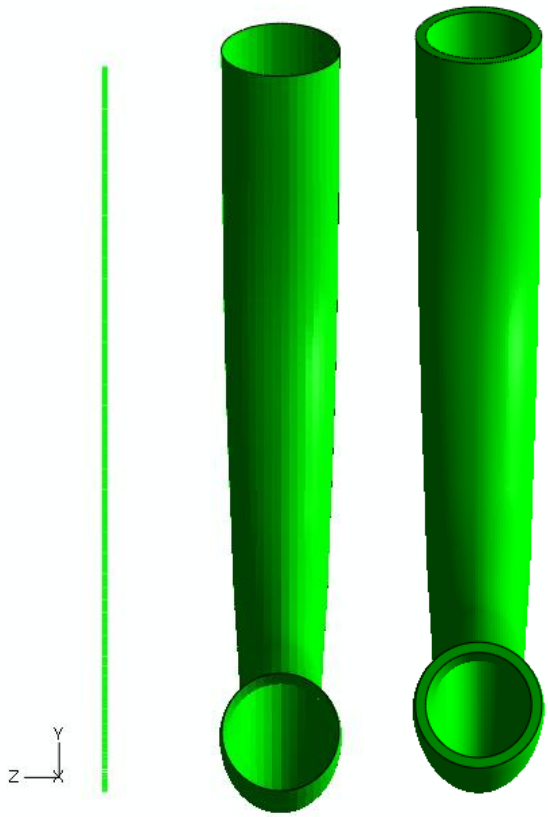

Figure 15. Mode 10 of different model types.

5 Dynamic analysis of a guillotine pipe break

A guillotine pipe break is chosen as a dynamic analysis case. It is first analysed using the combined model shown lowermost in Figure 3. That is a relatively large model using shell elements for the pipe (chosen based on the eigenfrequency results above) and solid volume elements for the concrete and the steel restraint. After that as a comparison, the same case is analyzed with a model using only elbow elements for the pipeline and a nonlinear spring element for the support. The properties such as the stiffness of the spring element are determined by preliminary static analyses with the large combined model.

A nonlinear spring element (SPRINGA) with a stiffness of 1 GN/m and a gap of 6 cm is chosen. The nonlinearity comes from the fact that the spring acts only in tension (when the pipe is moving downwards) and only after the gap has been closed. There is no plasticity, i.e. no irrecoverable deformation or displacement of the spring end points. The default tolerance parameter value of 0.03 for regularizing the material data is chosen. The spring is defined as follows:

```
*SPRING, RTOL=0.03, NONLINEAR, elset=springa
<blank line>
 0.,-0.5
 0.,0.
 0.,0.06
 100.e6,0.16
```

The release of fluid from a break in high-energy piping could result in significant changes in flow characteristic within the piping system, creating reaction forces, which dynamically excite the piping. If these forces are sufficient to cause pipe whip, nearby required systems must be protected or designed to withstand the consequences of a pipe whip. In reactor primary circuit, it is also important to keep the break flow area and thus the outflow of coolant limited in case of pipe break.

The fluid forces acting on the ruptured pipe are a function of time and space, and depend on the fluid state within the pipe prior to rupture, the break flow area, frictional losses, and plant system characteristics. Break flow area is often assumed to develop within one millisecond after break initiation. Fluid forces can be divided into two parts: initial thrust force and steady state thrust force. The former is:

$$F_{in} = P_0 A_e \qquad \text{(Equation 1)}$$

where P_0 is the initial pressure in the pipe and A_e the break plane area. The steady state thrust coefficient is dependent on the fluid state and the frictional effects. In this present case, the initial thrust force is approximately 9 MN.

Normally, a dynamic time history analysis shall be conducted of the ruptured piping to determine its response to the exciting forces. The pipe whip constraints and other objects that can modify the pipe whip motion shall be considered in the analysis. Absorption of energy via plastic pipe deformation is typically the most desirable method in the design of piping and restraints for protection against pipe whip effects. The elastic and plastic behaviour of the pipe material should be taken into account in the analysis (Vörös, 2002) (Micheli, 2003). More

about pipe breaks and the preliminary static analyses are reported earlier within this project (Calonius, 2008).

The analyses in this study consist of two steps. The first step is static during which an inner pressure is applied to the pipe. It is linearly ramped up in one second time. The upper end (called “free end” in this report) and the lower right end of the pipe are fixed during this step. The second step is dynamic with automatic time incrementation. Right in the beginning of it the free end is released, which initiates the pipe break condition. The same inner pressure remains throughout the second step even though in reality the pressure decreases at some rate when the water bursts out through the free end. Table 3 shows all the six dynamic analysis cases. Element, material and analysis types are varied. All the plastic analyses (SPI, SPE and EPI) were terminated before completion due to excessive deformation and exceeding of accuracy tolerance. The analyses lasted for from 5 minutes to 21 hours.

According to the results in the previous chapter, the best model using special-purpose elements for this purpose would have been the one with elbow elements in the bend and pipe elements in the straight parts of the pipeline. However, since the intention is to study the deformation of the pipe cross-section also near the restraint, a model with elbow elements for the whole pipeline section is used.

In the previous report (Calonius, 2008), only linearly elastic materials were used. Now, also plastic materials properties are used for the steel. The same steel material is used for the pipe and the restraint. The gap is included in the spring element, but after the gap is closed, the spring element behaves elastically. Thus, some clear differences in the behaviour of the restraint in these two model types are anticipated.

Only implicit scheme can be used for the direct time integration with elbow elements. For the sake of comparison, both implicit and explicit time integration in the case of the larger model.

Table 3. Dynamic analysis cases.

Case Code	Main element type	Main material type	Analysis type	Analysis time (dynamic step)	No. of time increments (dynamic step)	CPU time
SEI	shell	elastic	implicit	1 s	1 951	48 418 s
SEE	shell	elastic	explicit	1 s	451 742	25 491 s
SPI	shell	plastic	implicit	0.30 s	1 748	75 148 s
SPE	shell	plastic	explicit	0.26 s	329 457	22 887 s
EEI	elbow	elastic	implicit	2 s	949	565 s
EPI	elbow	plastic	implicit	0.22 s	330	274 s

Only some of the results are shown here. All the analyses were successful. The energy balance was mainly maintained and the results of shell and elbow models had a good correlation, with both plastic and elastic material properties. With plastic steel properties the plastic hinges formed in both models in a similar manner and in a realistic way. Also, stress results were in fairly good agreement. In elbow elements, stresses can be defined around the circumference of the pipe and through its wall thickness. The deformed shape of the cross-section is possible to be plotted as well.

Figure 16, Figure 17, Figure 18, Figure 19, Figure 20 and Figure 21 show the energy balance in all the cases. Energy balance is defined as (see the legend codes in above mentioned figures):

$$ETOTAL = ALLKE + ALLIE + ALLVD + ALLFD – ALLWK,$$

where ALLKE is kinetic energy, ALLIE is the strain energy, ALLVD is energy dissipated by viscous effects, ALLFD is energy dissipated through frictional effects and ALLWK is the external work done to the system.

$$ALLIE = ALLSE + ALLPD + ALLAE,$$

where ALLSE is recoverable strain energy, ALLPD is energy dissipated by plastic deformation and ALLAE is “artificial” strain energy associated with constraints used to remove singular modes (such as hourglass control) (Abaqus, 2007).

The balance is otherwise well maintained, except in case of implicit analyses with elastic steel properties (SEI and EEI), for some reason the total energy falls notably below zero. In case SEE, there is some “artificial” strain energy (ALLAE). However, the energy components behave quite similarly as a function of time in case of implicit and explicit time integration. In SEI the pipe hits the restraint 12 times during the dynamic step, whereas in SEE it hits the pipe 13 times. The external work (ALLWK) oscillates between approximately 1.4 MJ and 1.8 MJ is elastic cases and rises up to 44 MJ in the plastic case SPI.

Figure 22 shows the vertical displacement of the pipe at the restraint for cases SEI and EEI (elastic shell and elbow models with implicit direct time integration). They correspond with each other very well. The restraint forces were also similar. Figure 23 shows the vertical reaction force in the fixed pipe end in each case. Due to relatively large time interval of output points some peaks may be lost. In each case, this force rises to a positive value of approximately 0.2 MN during the first step (application of inner pressure). This means the pipe pushes downwards the fixed point. The force peaks are three times as high in elastic cases as they are in plastic cases (15 MN in comparison to 5 MN). That indicates how important it is to include plastic effects in simulations of pipe break scenarios especially with long pipe runs. When the pipe deforms even slightly but in several locations along the pipe, the force it actuates to the fixed end decreases considerably.

From the above mentioned results of the elastic models it can be concluded that the dominate vibration of the pipe has a frequency slightly over 11 Hz. That is naturally close to the eigenfrequency of a separate model of the pipeline. It seems that the impacts do not essentially affect the vibration frequency in the elastic model. The pipe vibrates dominantly according to its second mode and hits repeatedly the restraint near the highest point of its natural path (that would be unobstructed). Since the restraint or the pipe do not give in, there are only small displacements and the models are in good correlation with each other. From now on, only cases with plastic material properties are examined.

Figure 24 shows the deformed shapes in cases SPI and EPI 0.1 s after the pipe break. The plastic hinge has been formed in both cases. Maximum displacements are 3.18 m and 2.38 m, respectively. The results with explicit time integration corresponded to the ones with implicit integration, maximum displacement in the plastic analysis (SPE) after 0.1 s being 3.07 m. Figure 25 shows the vertical force in the free end of the pipe, in the fixed end of the pipe and in the spring or bottom of the concrete block in cases SPI and EPI. In both cases, the stress wave reaches the fixed end 2 ms and the pipe hits the restraint 17 ms after the pipe break. In case SPI, the steel restraint bends and gets very high plastic deformations. The pipe hits the edge of the concrete block 48 ms after the pipe break.

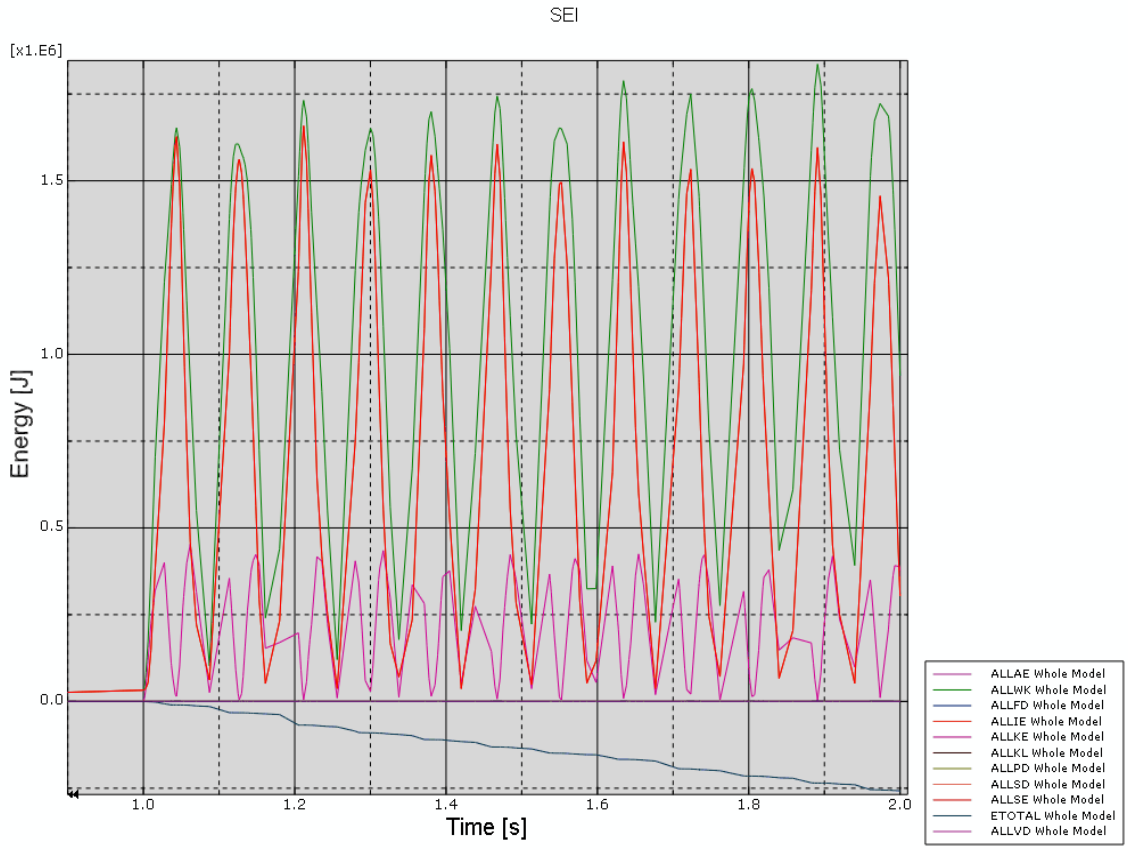

Figure 16. The energy [J] balance in case SEI.

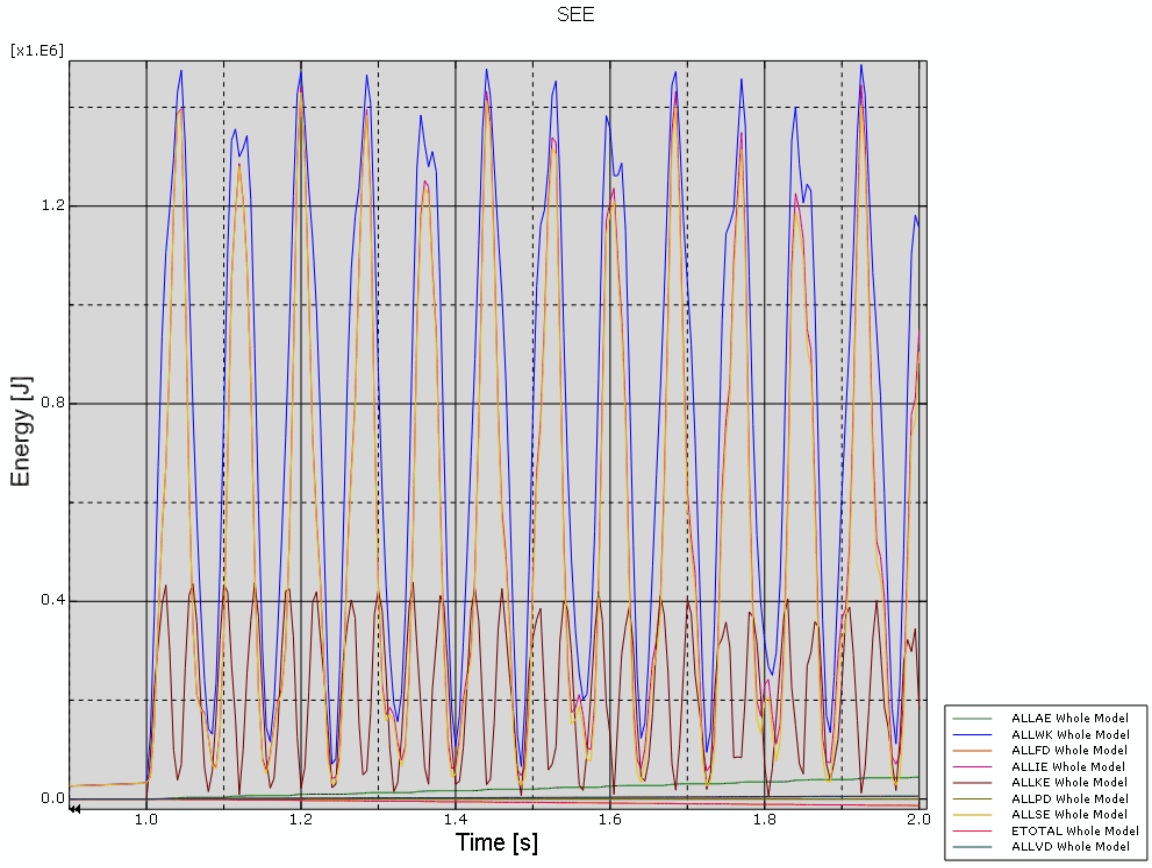

Figure 17. The energy [J] balance in case SEE.

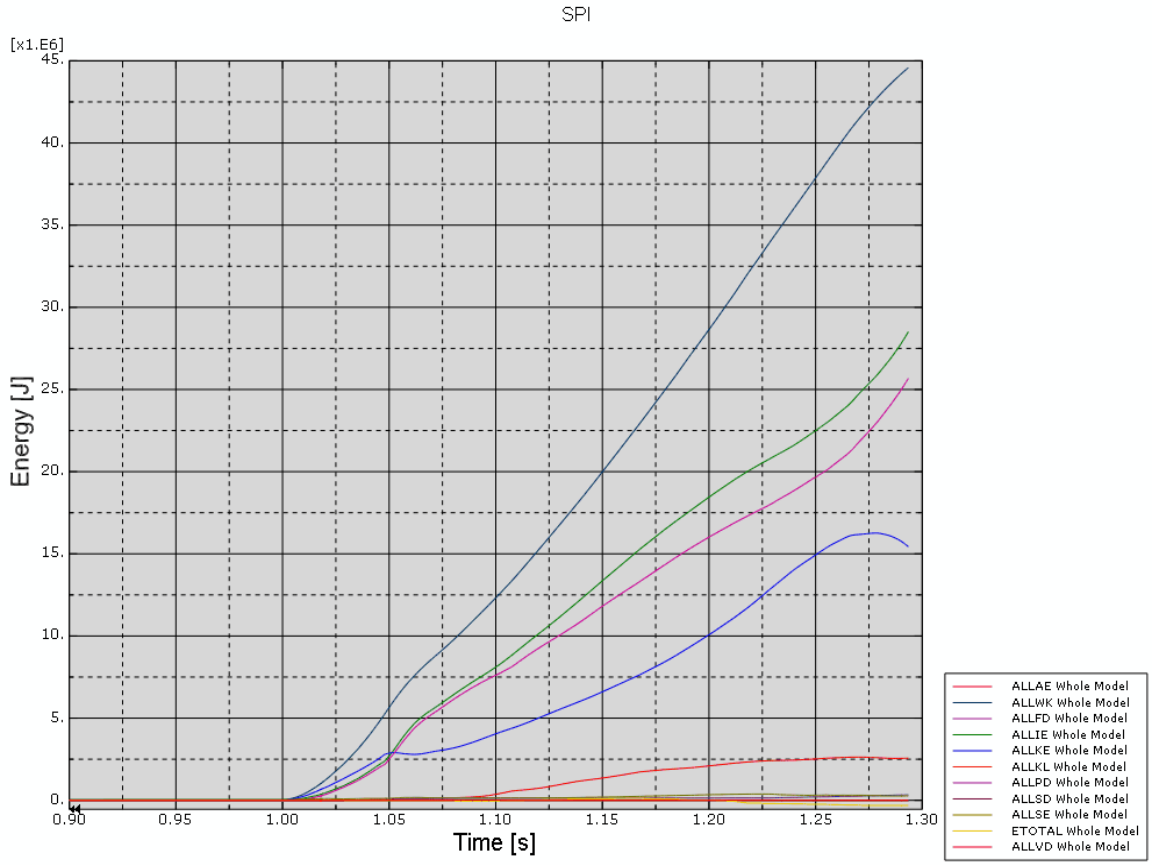

Figure 18. The energy [J] balance in case SPI.

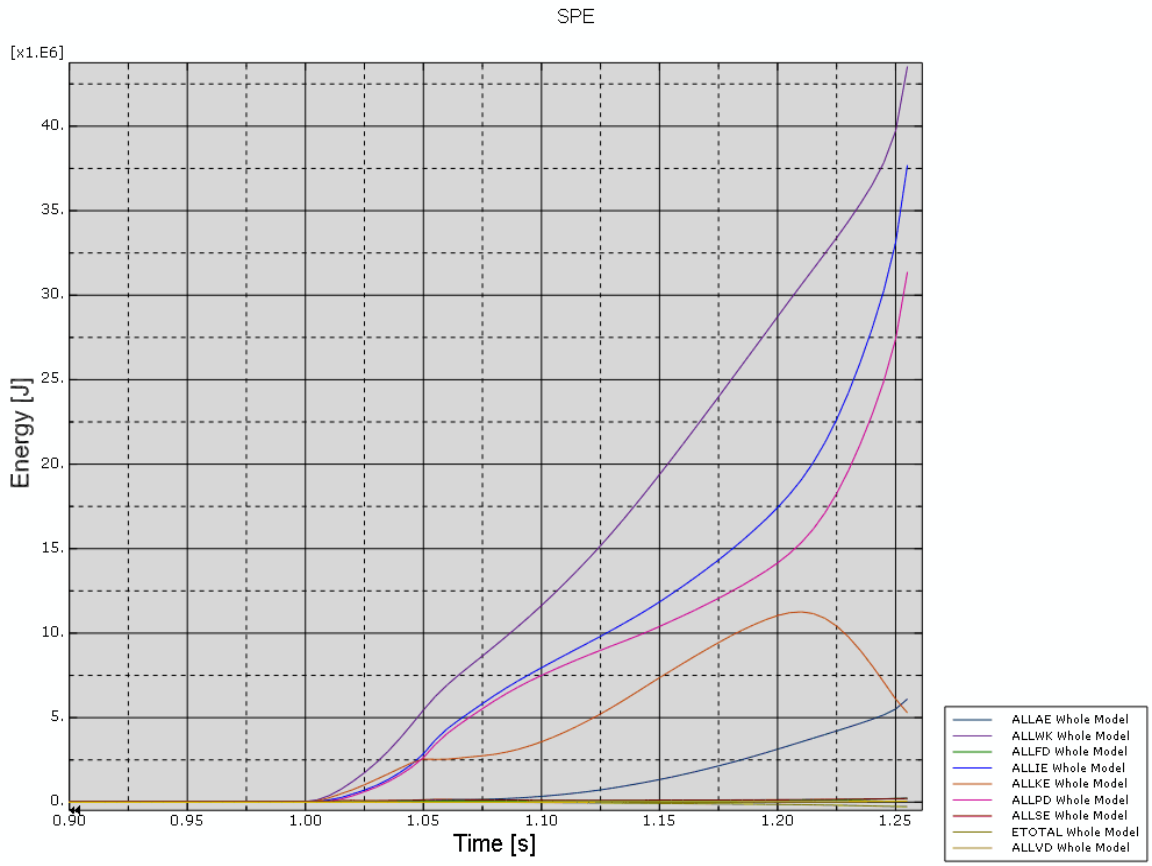

Figure 19. The energy [J] balance in case SPE.

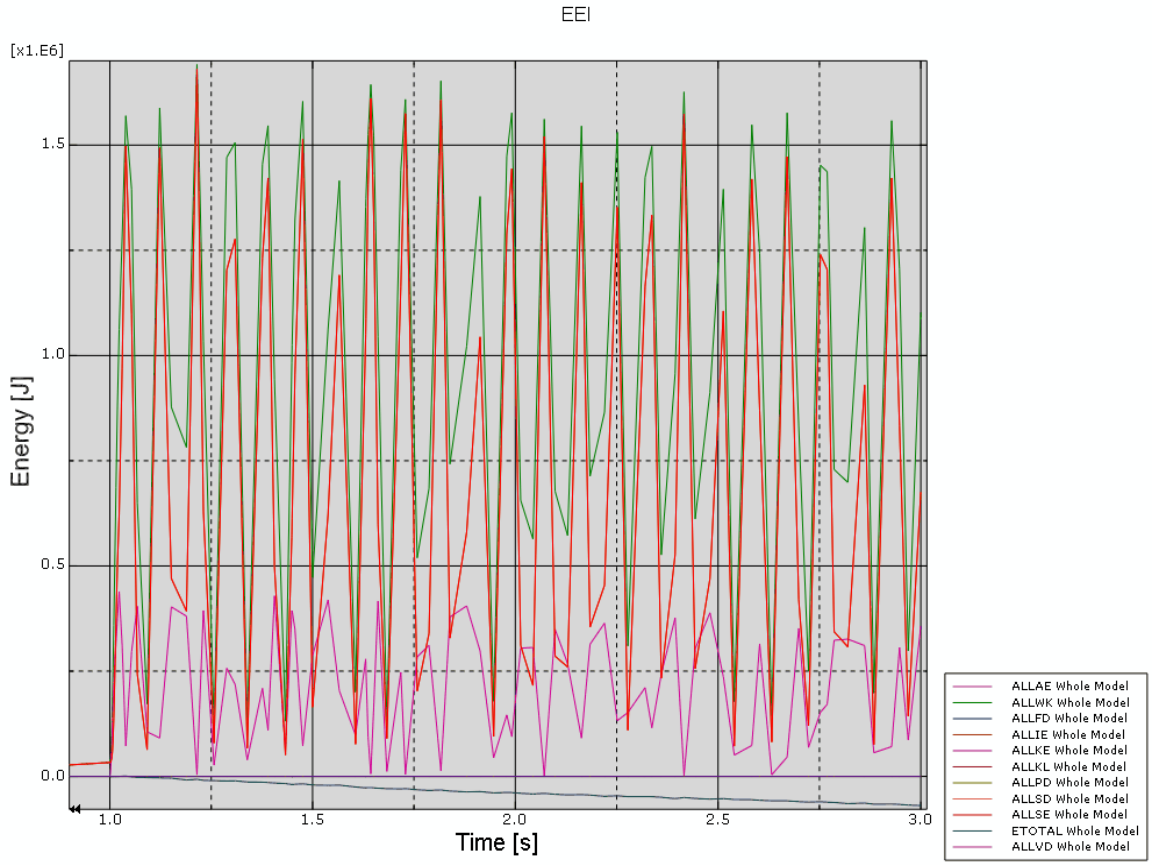

Figure 20. The energy [J] balance in case EEI.

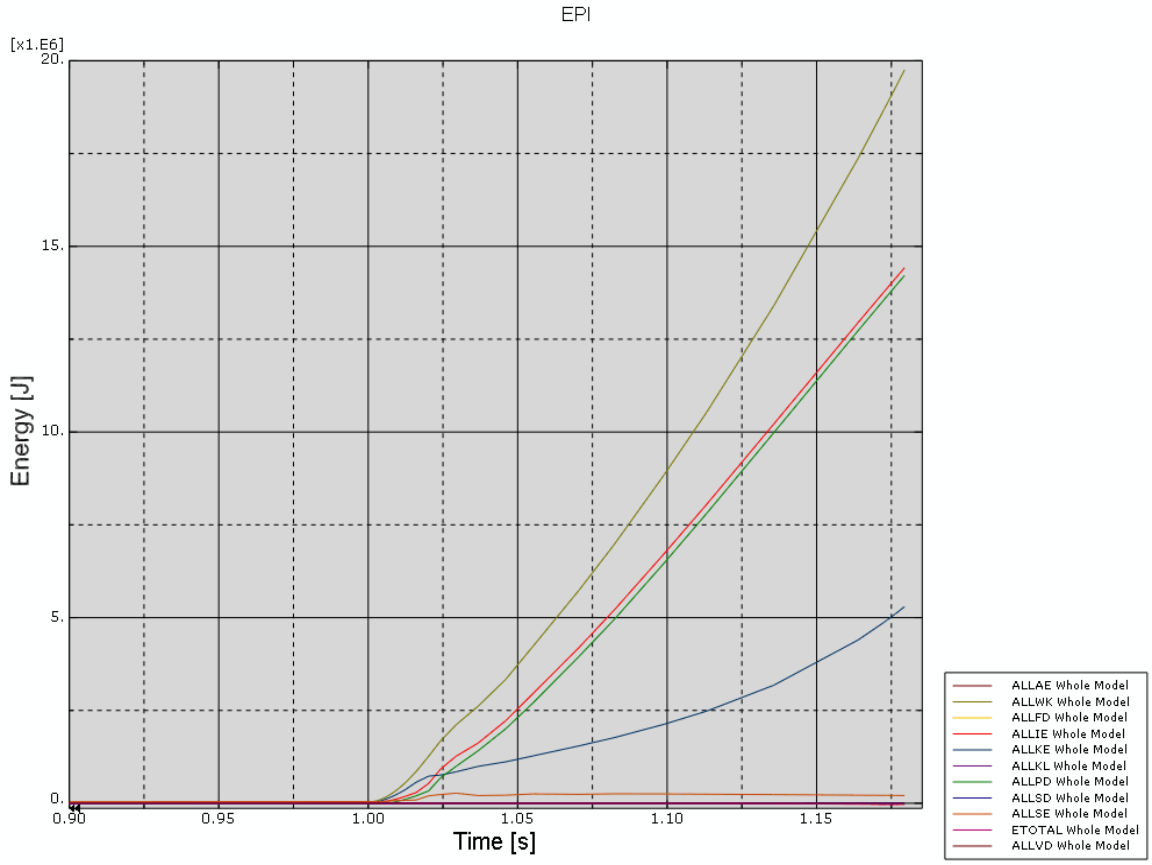

Figure 21. The energy [J] balance in case EPI.

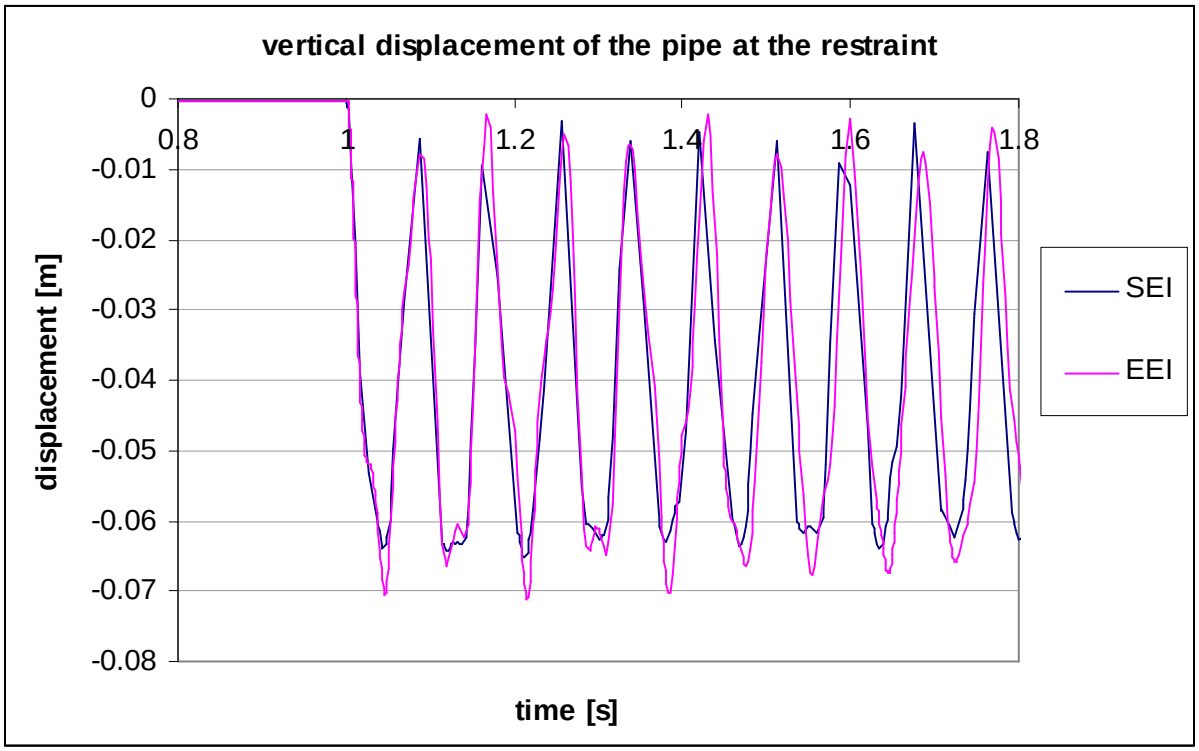

Figure 22. Vertical displacement [m] of the pipe at the restraint is cases SEI and EEI.

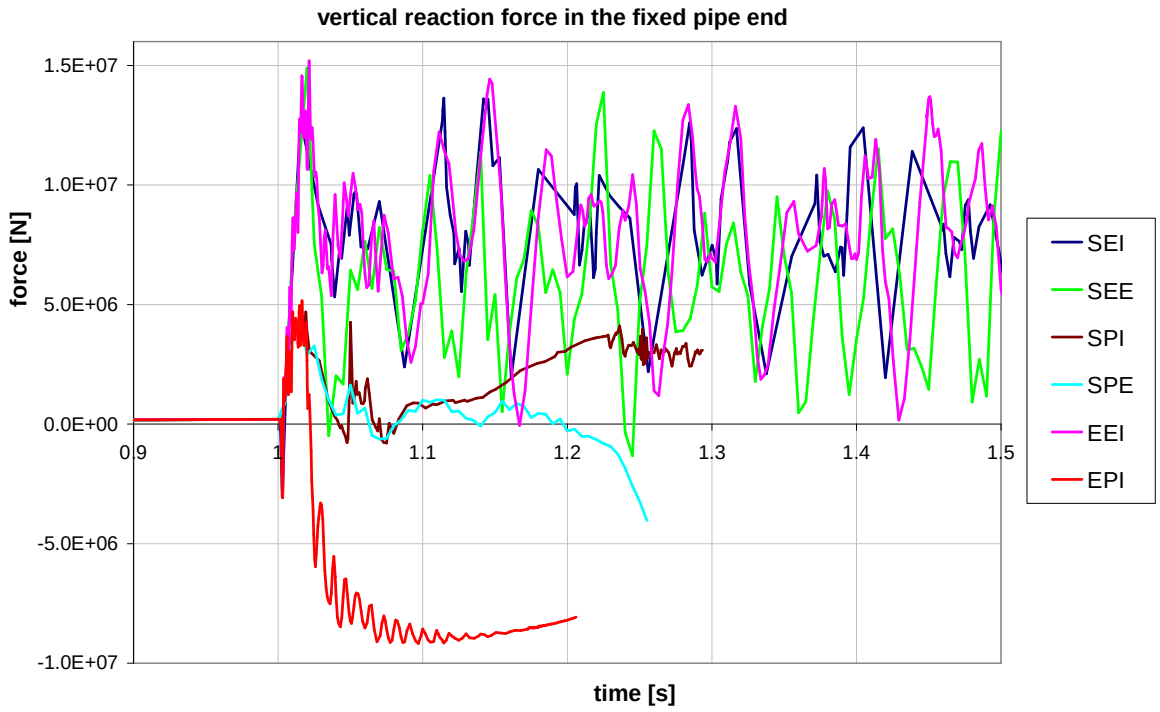

Figure 23. Vertical reaction force [N] in the fixed pipe end in each case.

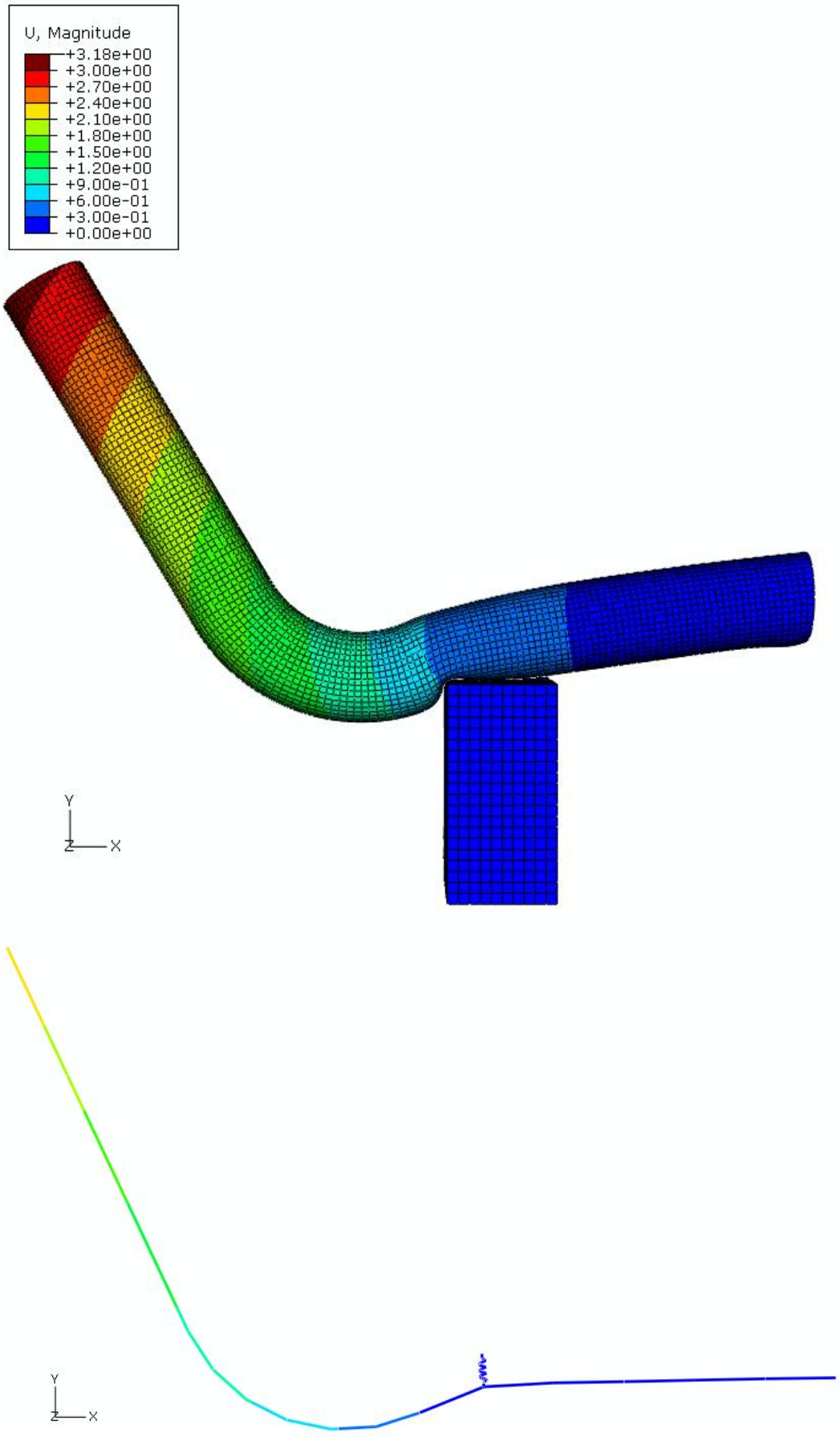

Figure 24. Deformed shape [m] of the models SPI and EPI 0.1 s after the pipe break.

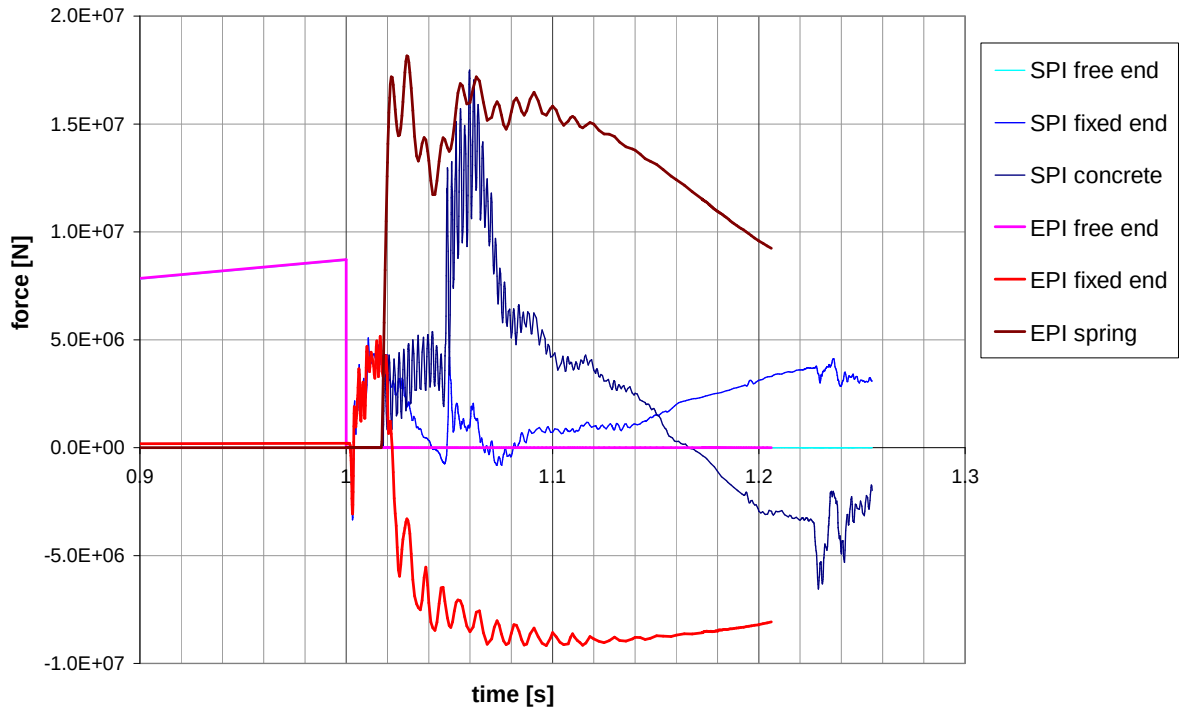

Figure 25. Vertical force [N] in the free end of the pipe, in the fixed end of the pipe and in the spring or bottom of the concrete block (cases SPI and EPI).

The deformed shape of the whole models SPI, SPE and EPI at time instants of 0, 0.06, 0.14 and 0.22 s (0.20 s for the case EPI) after the pipe break viewed from the side are shown in Figure 26, Figure 27 and Figure 28, respectively. The first plastic hinge develops to the fixed end at 0.02 s (plastic strain over 1% around the whole section), approximately at the same time when the pipe hits the restraint. The second hinge develops to the left side of the restraint at 0.07 s. After the pipe has hit the restraint, the main difference between the cases SPI and SPE (in addition to the type of the time integration) lies in the contact modelling. In case SPE, the contact is modelled more realistically with “general contact” feature offered by Abaqus which applies contact conditions between all surfaces in the model and allows the self contact within each surface. In case SPI, only the most relevant contacts are modelled, and the pipe can move more freely. This can clearly be seen in the deformed shapes. The element number 6 is coloured red in Figure 28. The corresponding elements are also coloured red in the shell element model.

The elbow element model behaves in a very similar manner at least in the global sense. The spring element models quite realistically the restraint and the plastic hinge is formed. However, the stress distribution and deformation of the cross section near the restraint have to differ somewhat from the ones in the shell element model. That is studied in more detail below.

Figure 29, Figure 30 and Figure 31 show the cross sections viewed horizontally from fixed pipe end at time instants of 0.06 s, 0.14 s and 0.22 s after the pipe break, respectively. The undeformed shape is also shown. The location is slightly left from the restraint (coloured red in the deformed shape plots of whole models). The implicit analysis result (SPI) is shown on the left and the explicit analysis result (SPE) on the right in these figures. In case SPI, the cross-section gets larger deformations. That is at least partly due to the different contact conditions.

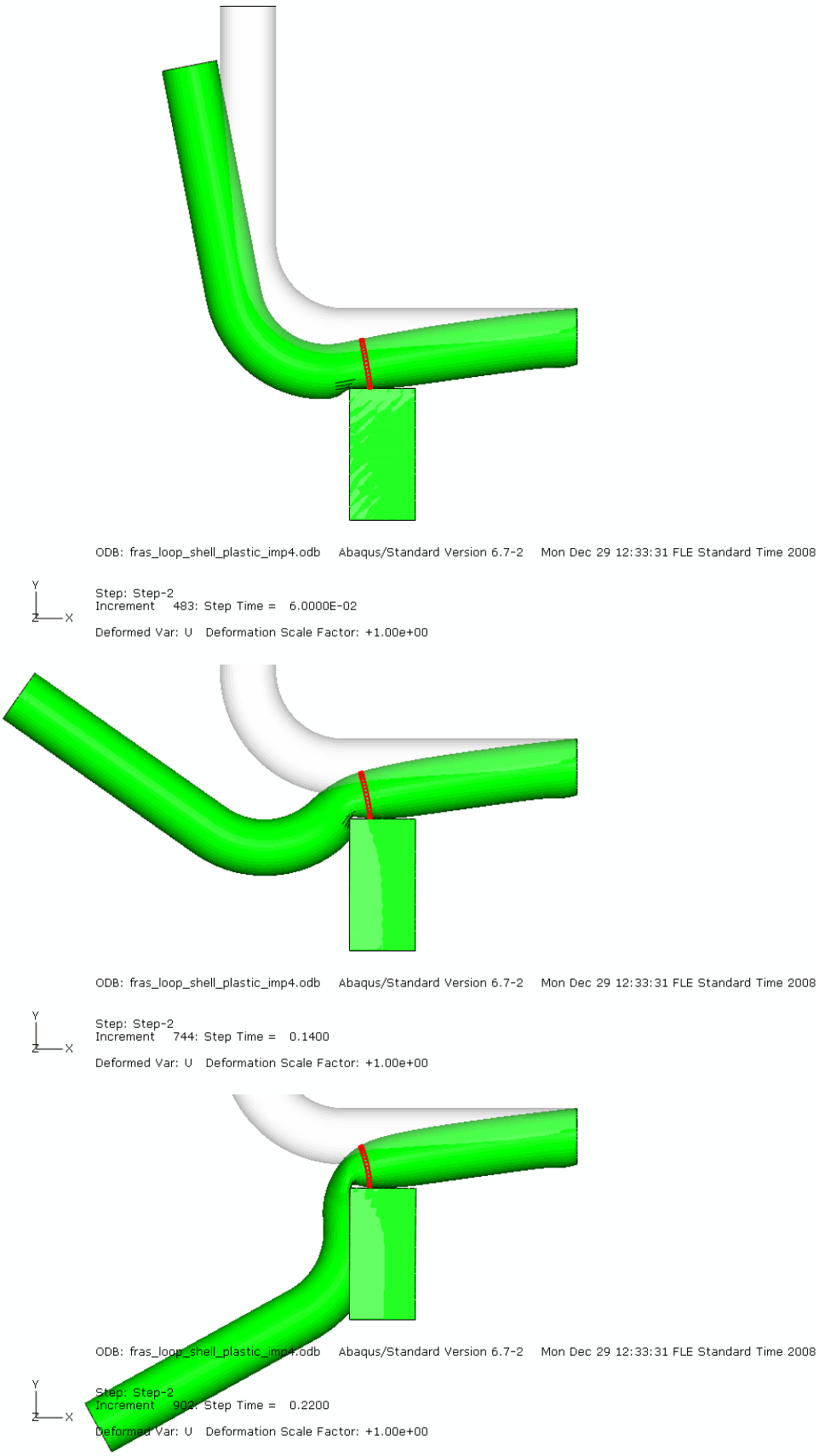

Figure 26. The deformed shape of the whole model SPI at time instants of 0.06, 0.14 and 0.22 s after the pipe break viewed from the side.

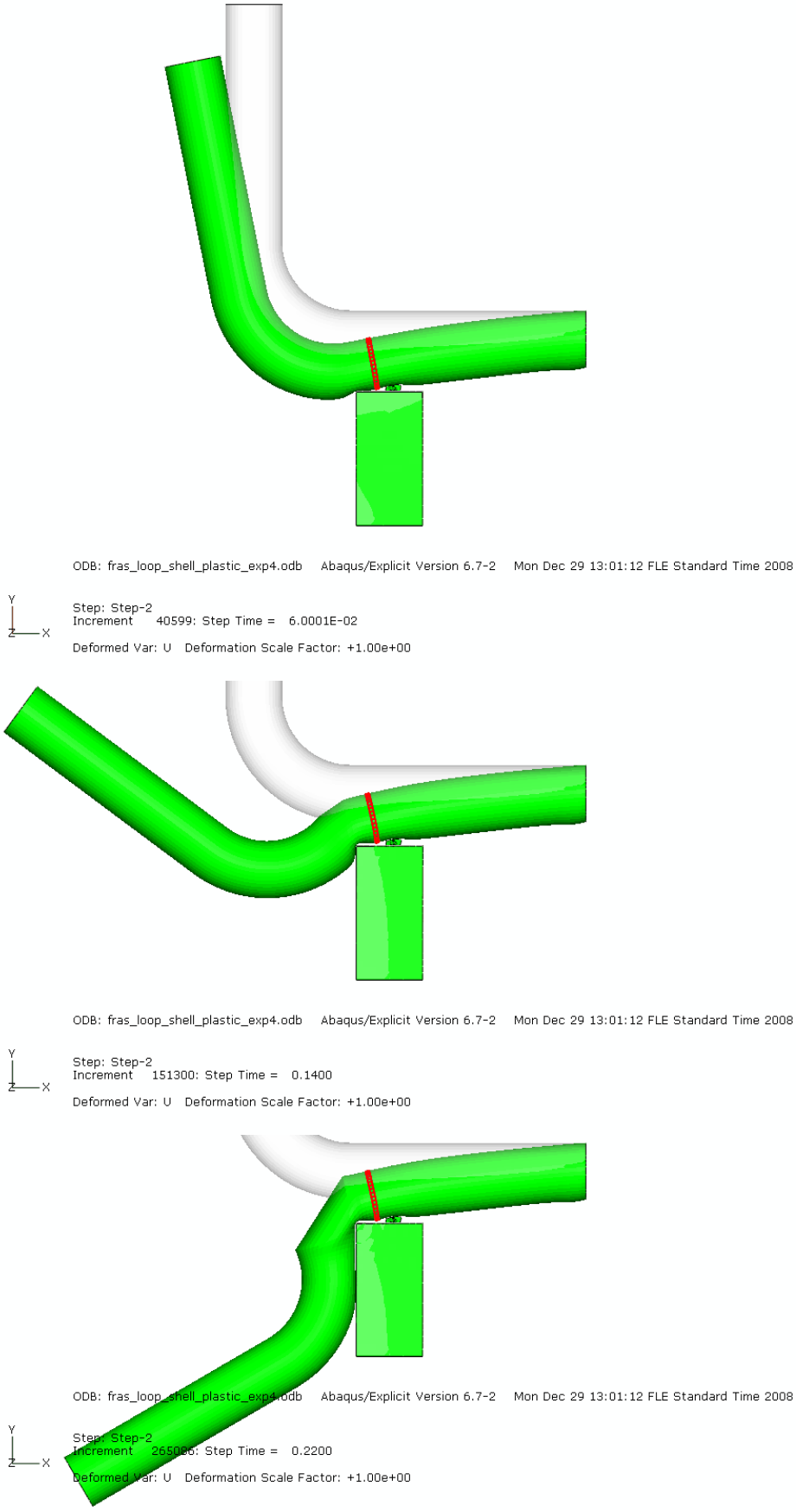

Figure 27. The deformed shape of the whole model SPE at time instants of 0.06, 0.14 and 0.22 s after the pipe break viewed from the side.

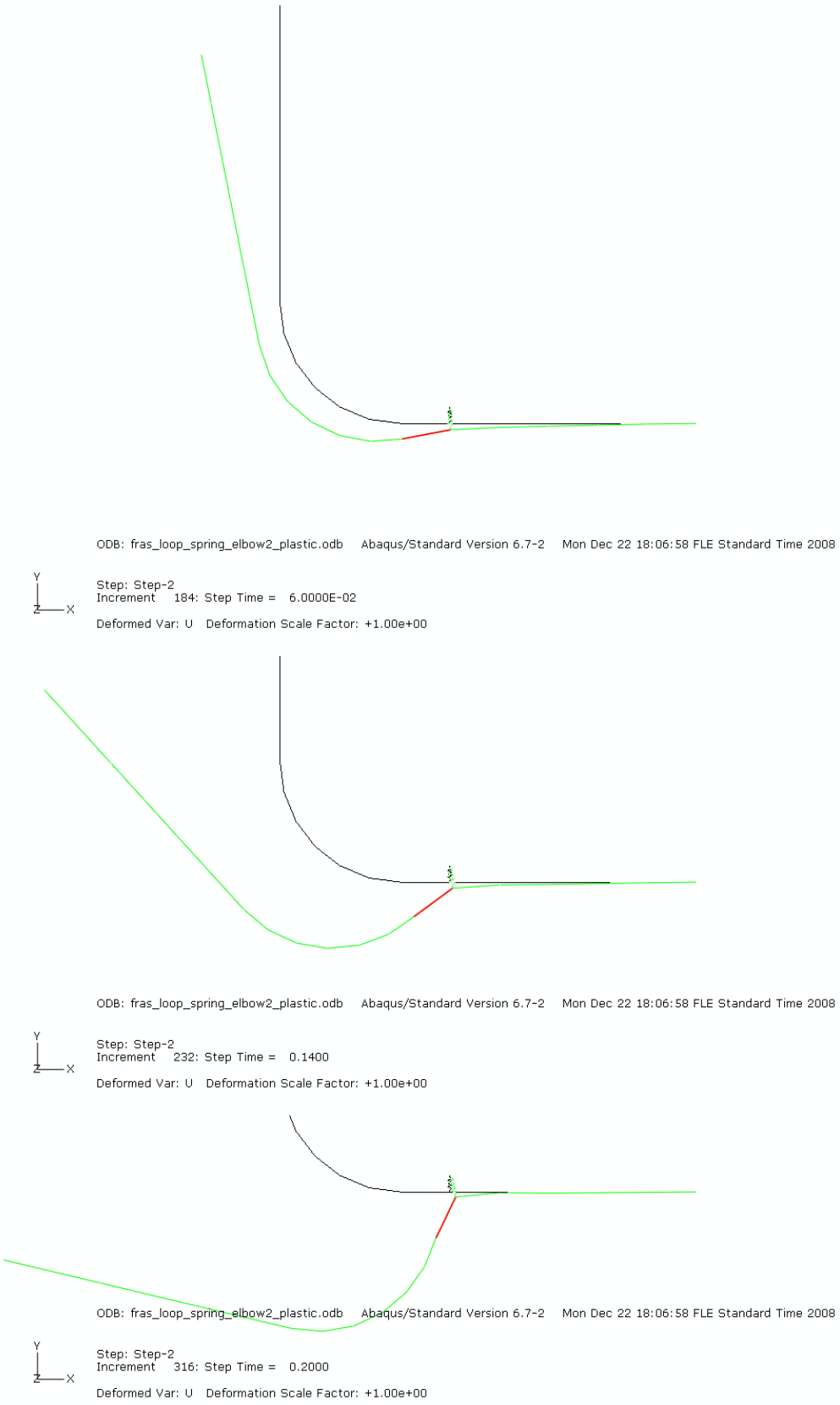

Figure 28. The deformed shape of the whole model EPI at time instants of 0.06, 0.14 and 0.20 s after the pipe break viewed from the side.

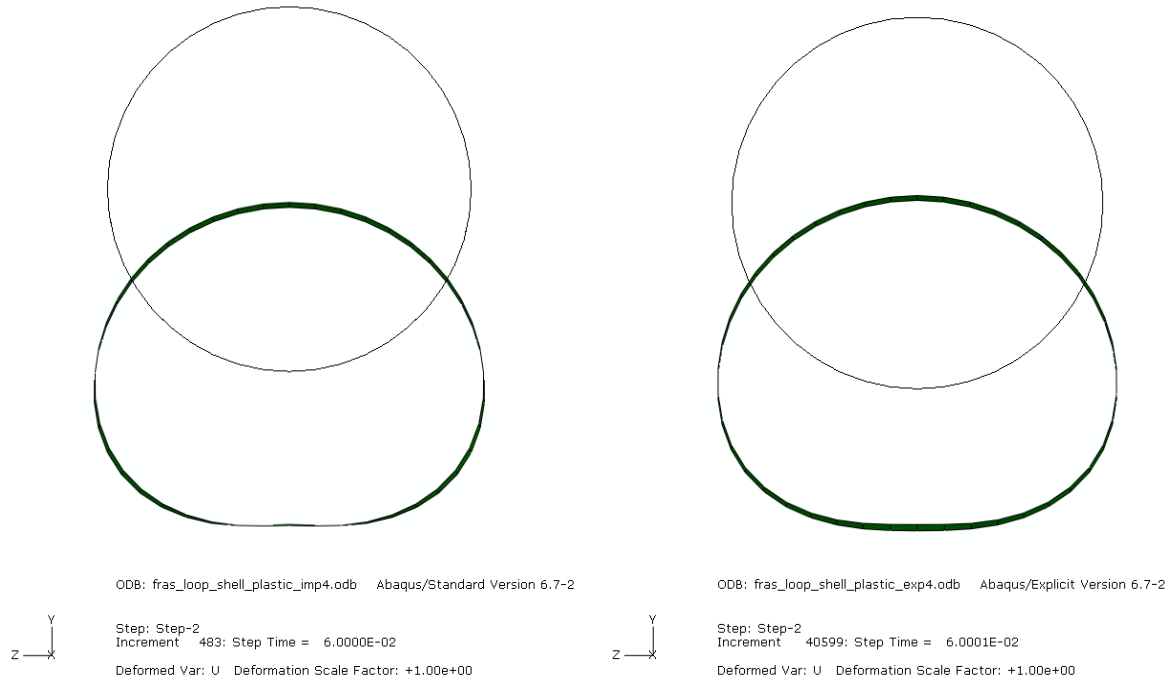

Figure 29. Cross-sections at time instants 0 and 0.6 s after the pipe break at the position slightly left from the restraint. The implicit analysis result (SPI) on the left, explicit on the right (SPE).

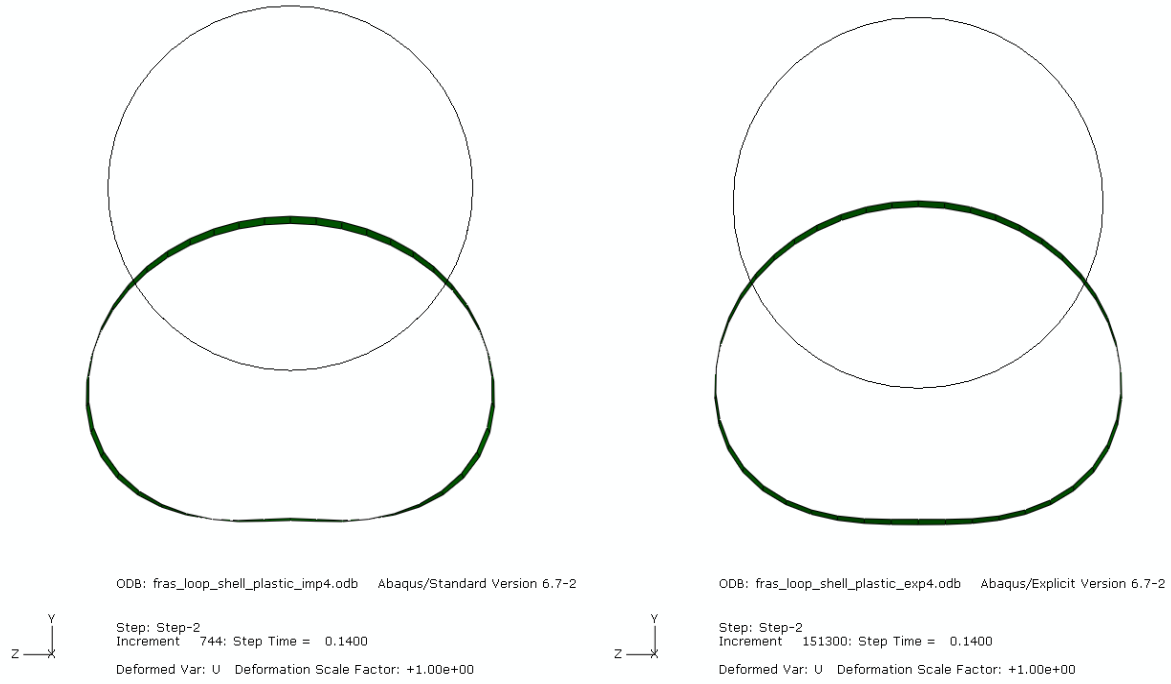

Figure 30. Cross-sections at time instants 0 and 0.14 s after the pipe break at the position slightly left from the restraint. The implicit analysis result (SPI) on the left, explicit on the right (SPE).

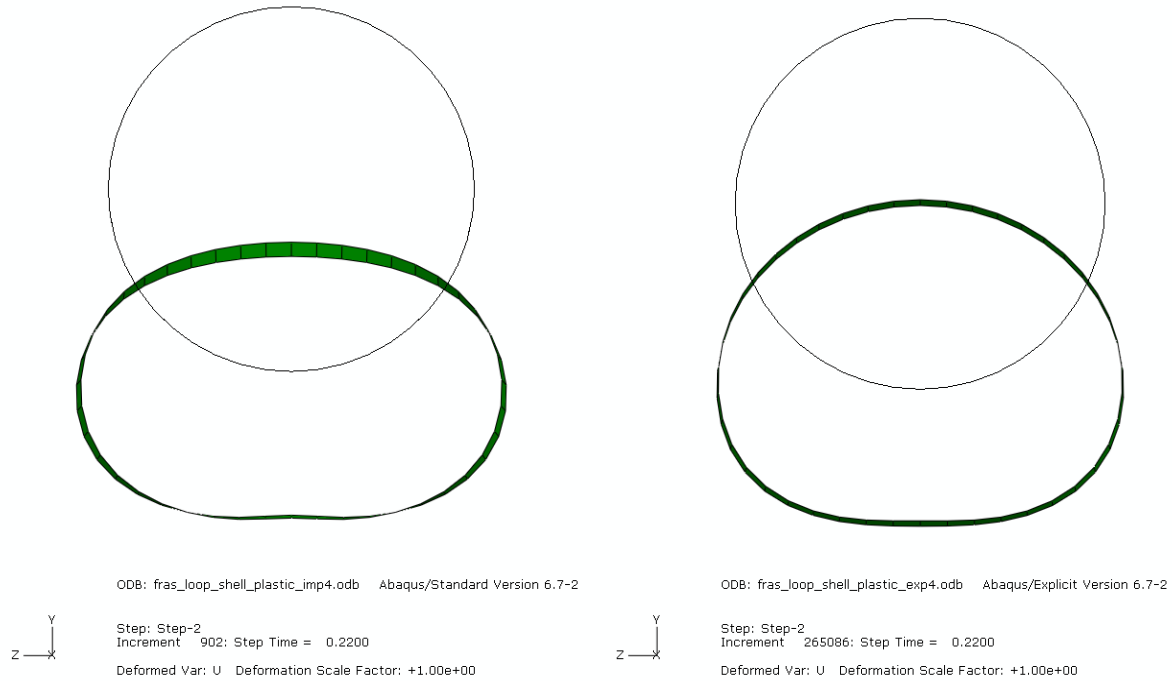

Figure 31. Cross-sections at time instants 0 and 0.22 s after the pipe break at the position slightly left from the restraint. The implicit analysis result (SPI) on the left, explicit on the right (SPE).

The deformed shapes of the pipe cross-section 0.3 m left from the restraint in model EPI at time instants of 0, 0.06, 0.14 and 0.22 s after the pipe break are shown in Figure 32. The colour changes from dark blue to red in time. These shapes are plotted from the coordinate values (COORD in Abaqus) of the first element left of the restraint (element number 6 in Figure 4). These values are from the middle of the elbow element lengthwise and from 20 points around the circumference of the pipe wall. Thus, it is impossible to get directly the deformed shape exactly at the location of the spring element. Also, the spring element cannot be fixed to any of those points around the pipe cross-section but only to an imaginary middle point of the cross-section. That is one of the reasons the deformation of the cross-section cannot be modelled very accurately with elbow elements near these kinds of supports. In spite of that, the behaviour of the cross-section corresponds well to the one of the shell element model.

The current release of Abaqus/Standard does not provide a direct way of visualizing the cross-section ovalization. However, the utility routine felbow.f creates a data file that can be used in Abaqus/CAE to plot the current coordinates of the integration points around the circumference of the elbow section of interest. The routine uses output variable COORD to obtain the current coordinates of the integration points. These values are available only if geometric nonlinearity is considered in the step. The routine is suitable for elbow elements oriented arbitrarily in space: the integration points of the elbow section are projected appropriately to a coordinate system suitable for plotting the cross-section. In addition to facilitating the visualization of the cross-section ovalization, the program also allows you to create data files to plot the variation of a variable along a line of elbow elements and around the circumference of a given elbow element. For some reason yet unknown, this routine did not work. Instead, the numerical results were transferred to Excel programme and plotted there. The COORD values were not projected in the above mentioned manner.

All the cross-section deformation results shown are taken from the corresponding locations and time instants in each of the three models and are thus comparable. The elements from which the results are taken are shown in red colour in Figure 26, Figure 27 and Figure 28.

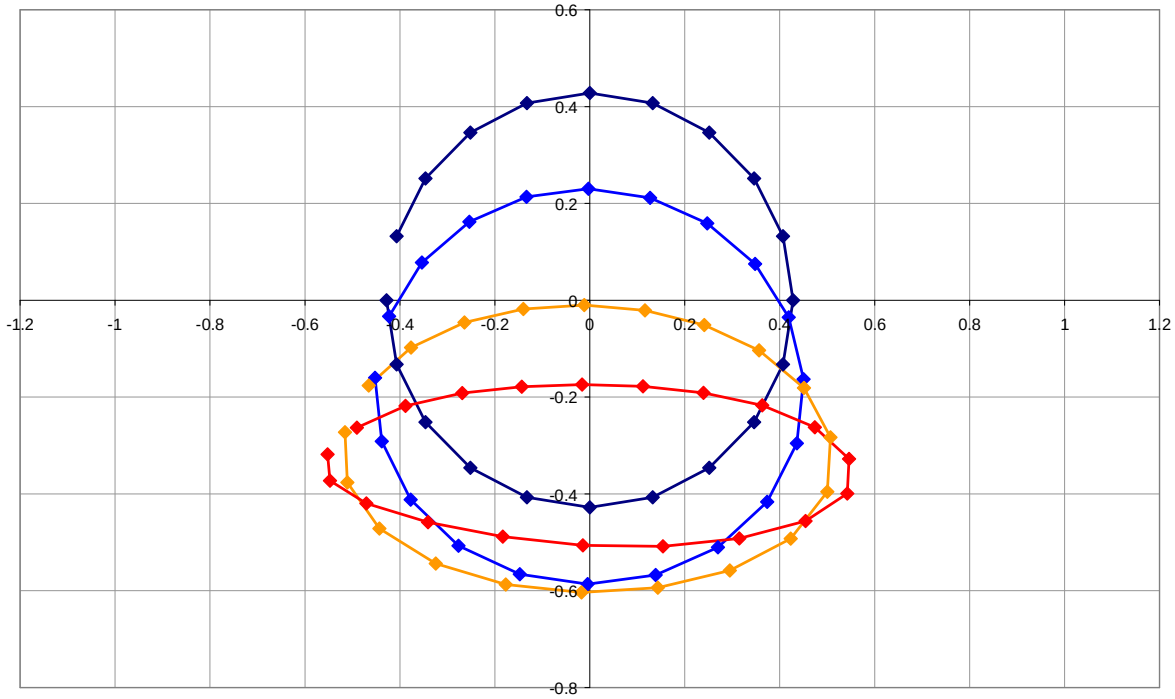

Figure 32. Cross-sections at time instants 0 (dark blue), 0.06 (light blue), 0.14 (orange) and 0.22 s (red) after the pipe break at the position slightly left from the restraint (EPI). The origin is the midpoint of the cross-section in its initial position [m].

Next, the stress values in the pipe wall are examined. Only cases SPI and EPI are compared with each other. Since the deformations are really large near the restraint and the contact and boundary conditions are different, it is more convenient to examine the stresses somewhere at the bend. Unfortunately, the shell element directions 1 and 2 are reversed along the bend when moving from the horizontal part to the vertical part and the stresses are difficult to be compared with the ones of the elbow model. Three cross-sections are chosen. They are the elbow elements 5, 6 and 9 (see Figure 4). They lie in both sides of the restraint and near the middle of the bend.

Figure 33 shows, how the elbow elements are specified. There are 20 integration points around the section and five thickness direction integration points at each such point, with point 1 on the inside surface of the pipe and point 5 on the outside surface. The extrados and intrados are the sides of the pipe bend that are furthest away from centre and closest to the centre of the torus, respectively.

Figure 34 shows the material orientation in the shell element model. The whole model is shown above and the three examined cross-sections below. The situation is easy near the restraint but troublesome in the bend. The 1-axis and 2-axis are not following the main directions of the pipe and do not thus correspond completely to the ones in the elbow element model.

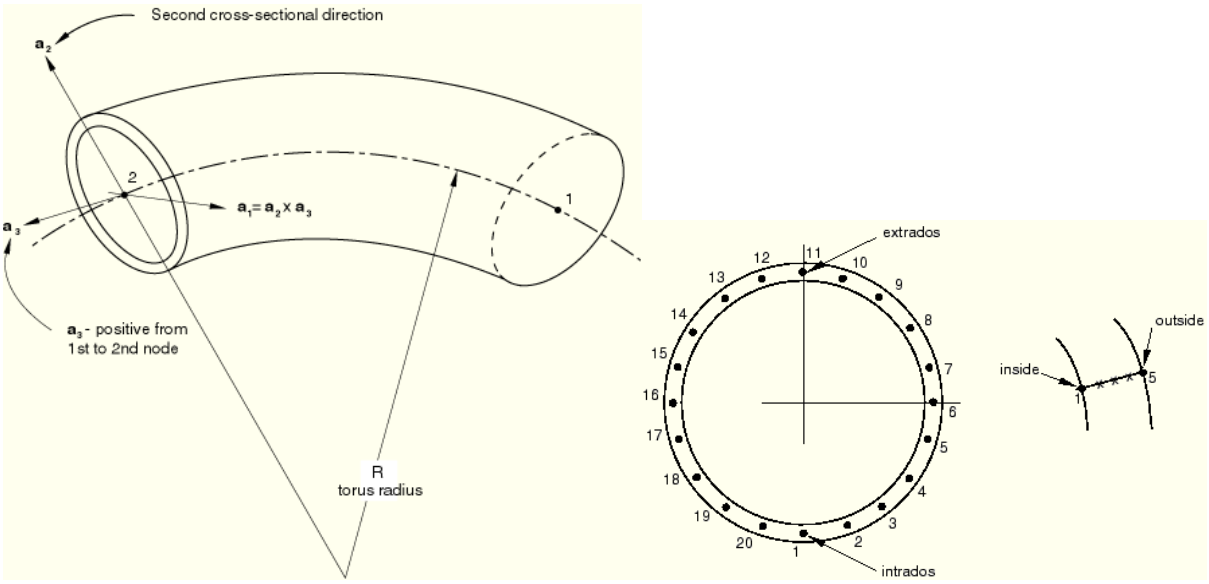

Figure 33. Specifying an elbow element.

First, the stress distributions in the whole shell element model are shown in order to get a better idea of the stress fluctuations during the pipe break. Figure 35 shows the S11 stresses on the outer surface just before the pipe break and at 0.06 s after it. S11 is the axial stress in the horizontal part of the pipe and the hoop stress in the vertical part. Figure 36 shows the same stress distribution at 0.14 s and 0.20 s after the pipe break. Figure 37 and Figure 38 show the corresponding S22 results. S22 is the hoop stress in the horizontal part of the pipe and the axial stress in the vertical part.

In the next figures, the x-axis represents the radial angle in which 0 degrees is the bottom of the pipe and the extrados in the bend, 180 degrees is the top of the pipe and the intrados in the bend etc. The y-axis represents the stress value and the range is from 300 MPa compression to 300 MPa tension in each figure. Remember, that the yield stress is 210 MPa. Figure 39 shows the axial stress on the outer surface around the cross-section 0.3 m right from the support (cases SPI and EPI). Figure 40 shows the axial stress on the outer surface around the cross-section 0.3 m left from the support (cases SPI and EPI). Figure 41 shows the axial stress (or S11 in case SPI) on the outer surface around the cross-section near the middle of the bend (cases SPI and EPI). Figure 42 shows the hoop stress on the outer surface around the cross-section 0.3 m right from the support (cases SPI and EPI).

Figure 43 shows the hoop stresses on the outer surface around the section 0.3 m right from the support as functions of time (cases SPI and EPI). The stress magnitudes are lower in elbow element model. Figure 44 shows the hoop stress on the outer surface around the cross-section 0.3 m left from the support (case EPI). Figure 45 shows the hoop stress on the outer surface around the cross-section near the middle of the bend (case EPI).

There are some clear differences in the stress distributions of shell and elbow element models, but in general level the elbow element describes reasonably well the stress distribution. After the static step, the stress distributions of shell and elbow element models are in very good agreement.

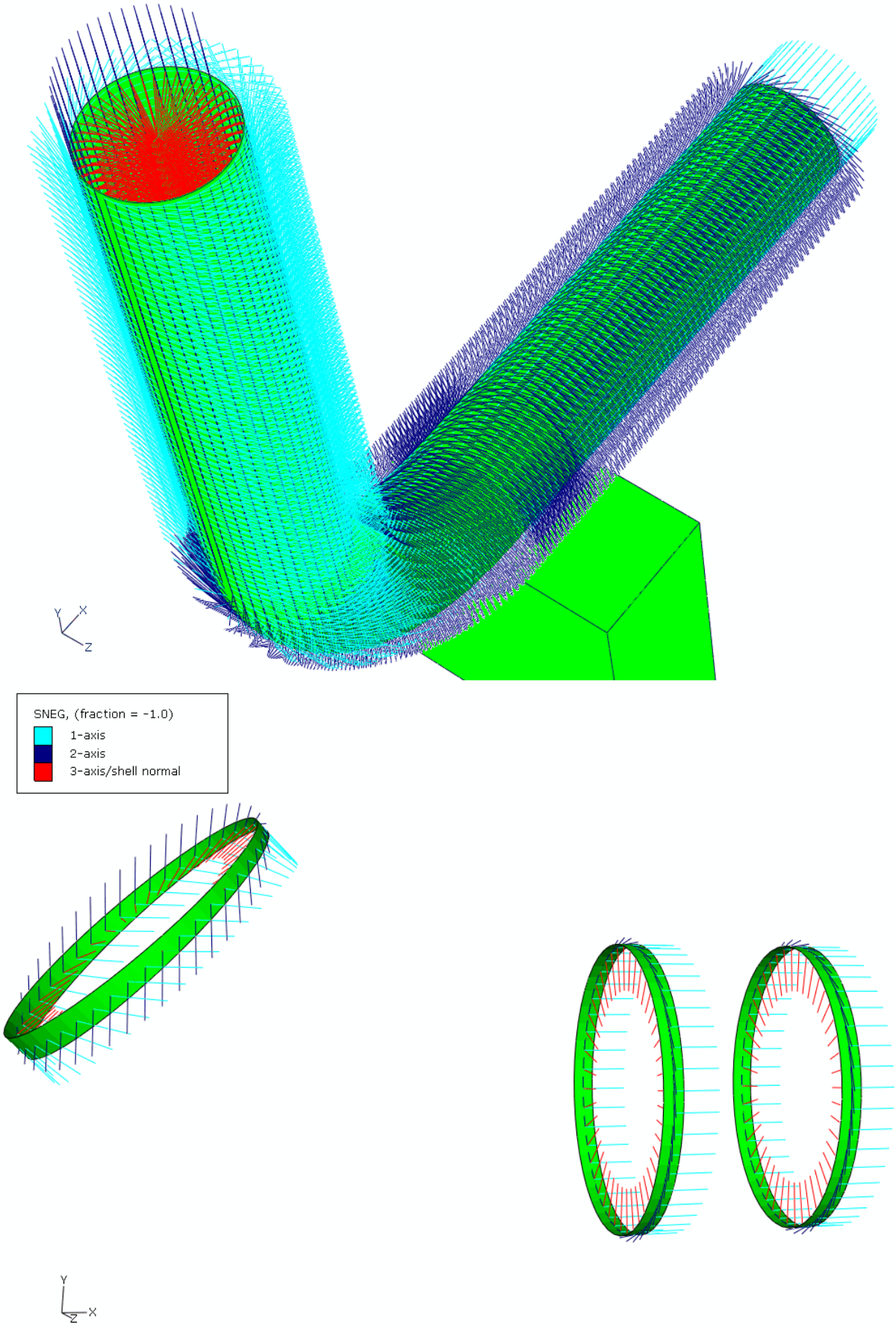

Figure 34. The material orientation in the shell element model.

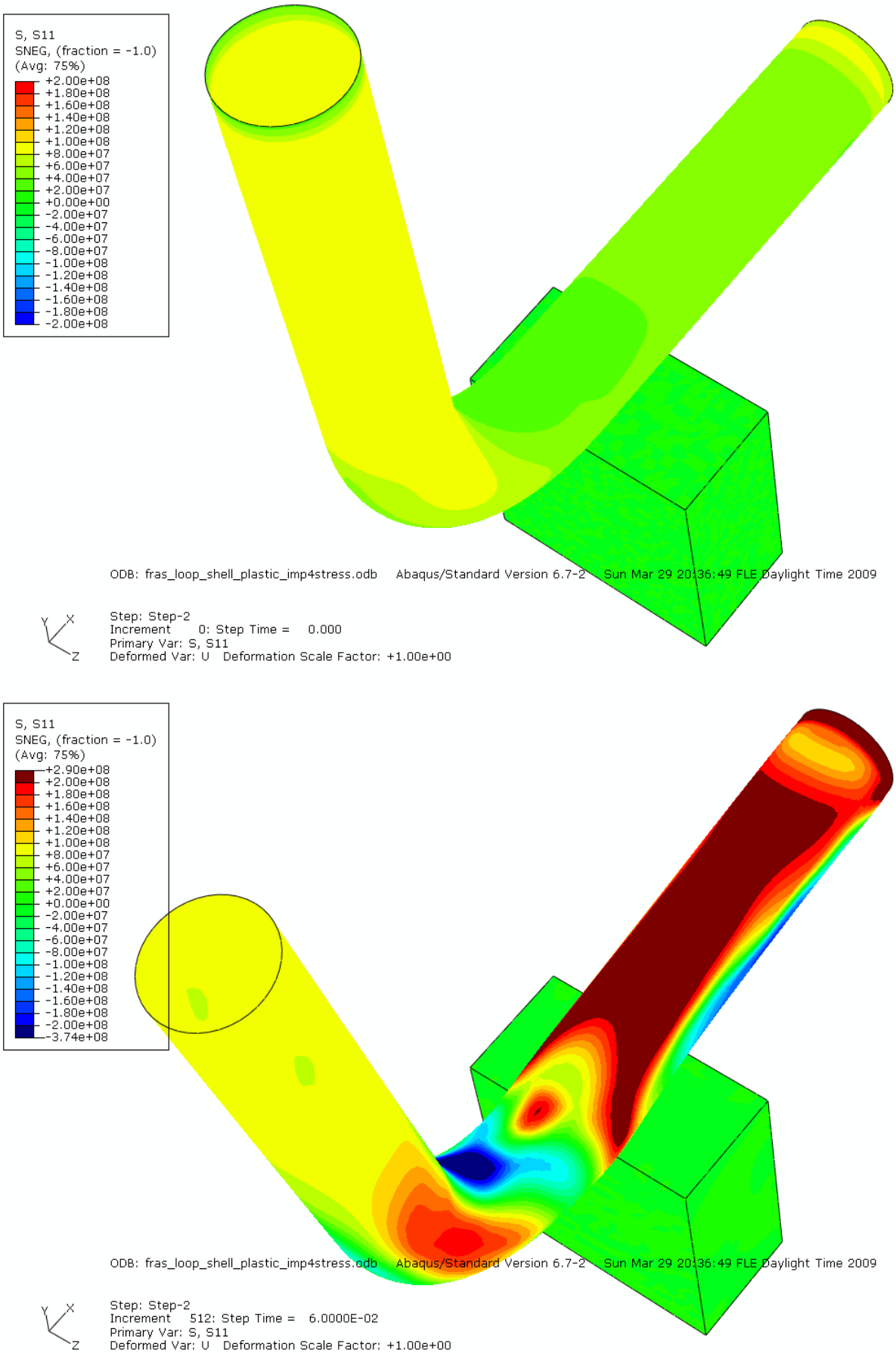

Figure 35. S11 [Pa] on the outer surface just before the pipe break and at 0.06 s after it.

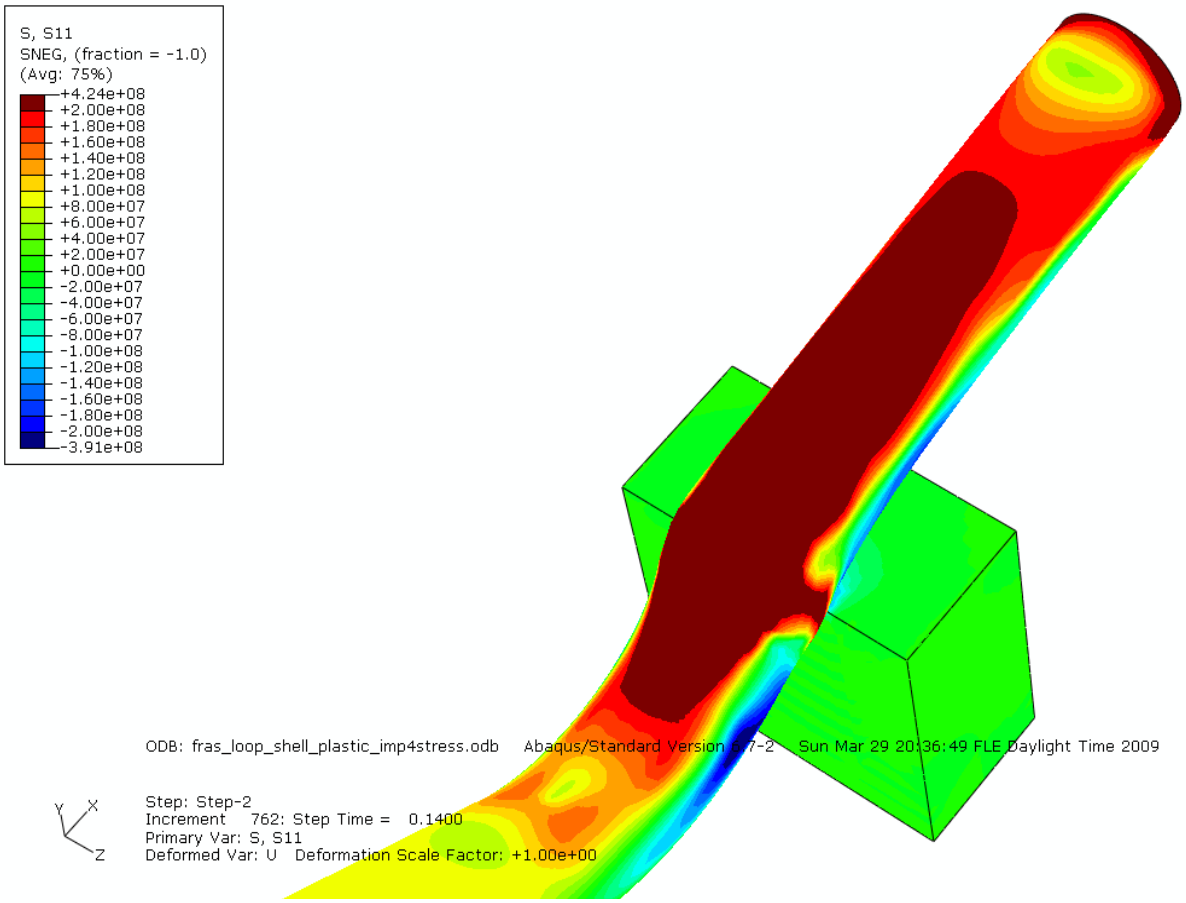

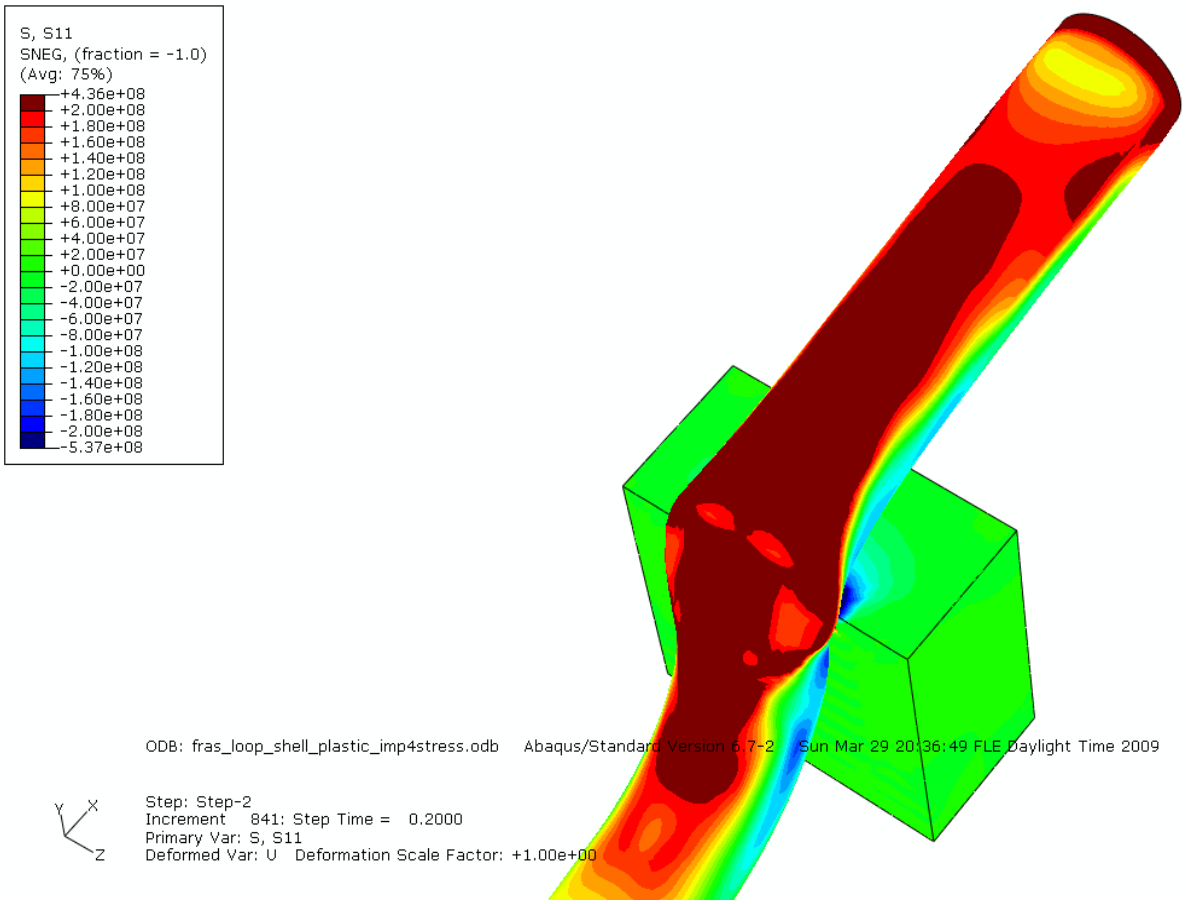

Figure 36. S11 [Pa] on the outer surface at 0.14 s and 0.20 s after the pipe break.

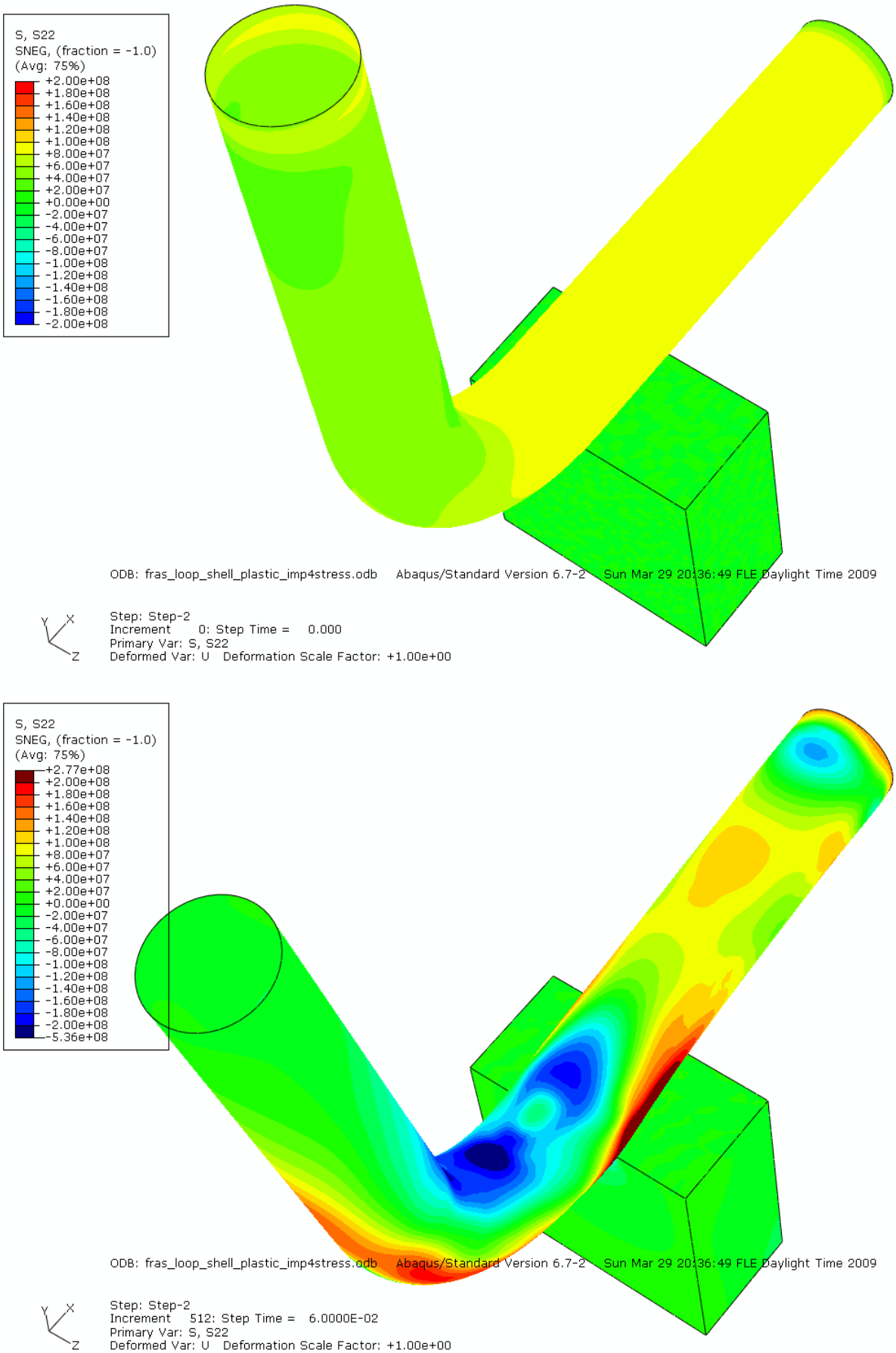

Figure 37. S22 [Pa] on the outer surface just before the pipe break and at 0.06 s after it.

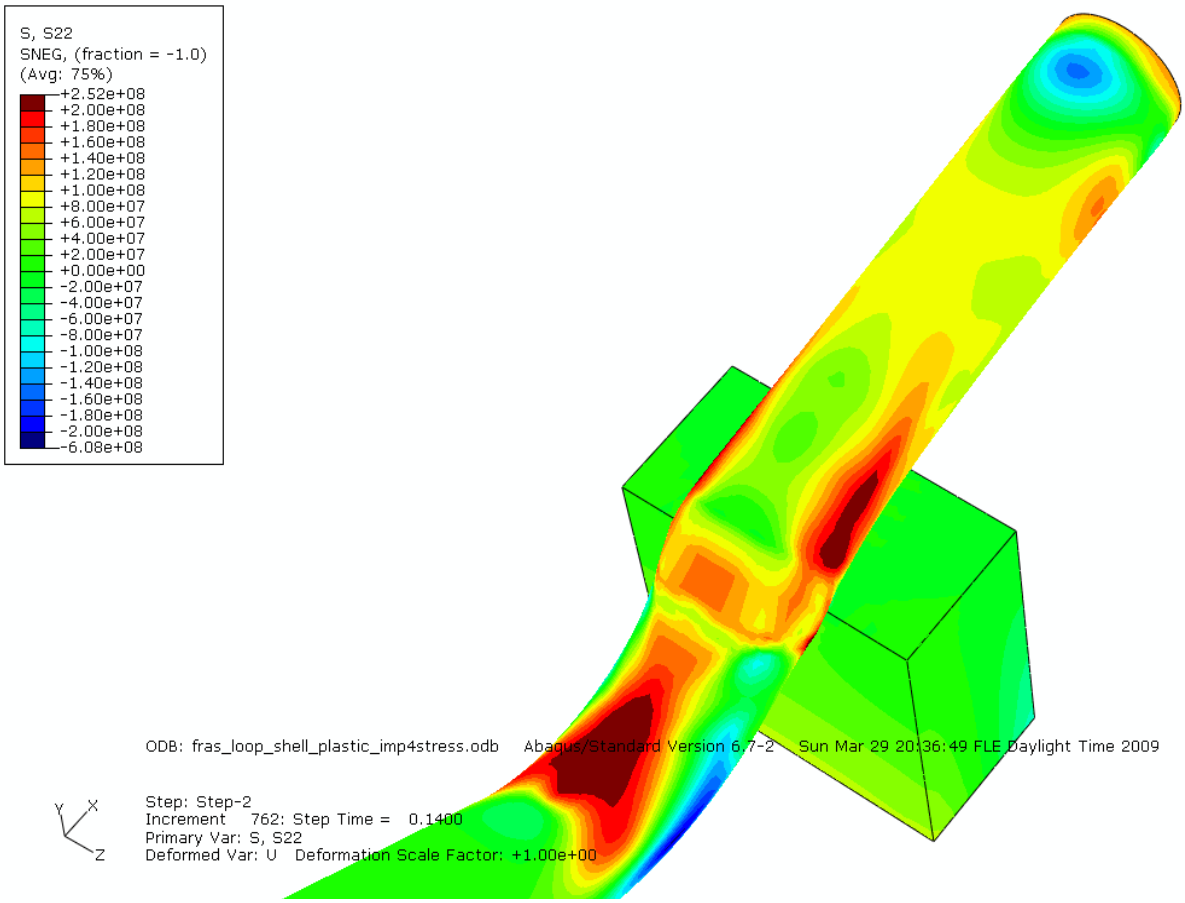

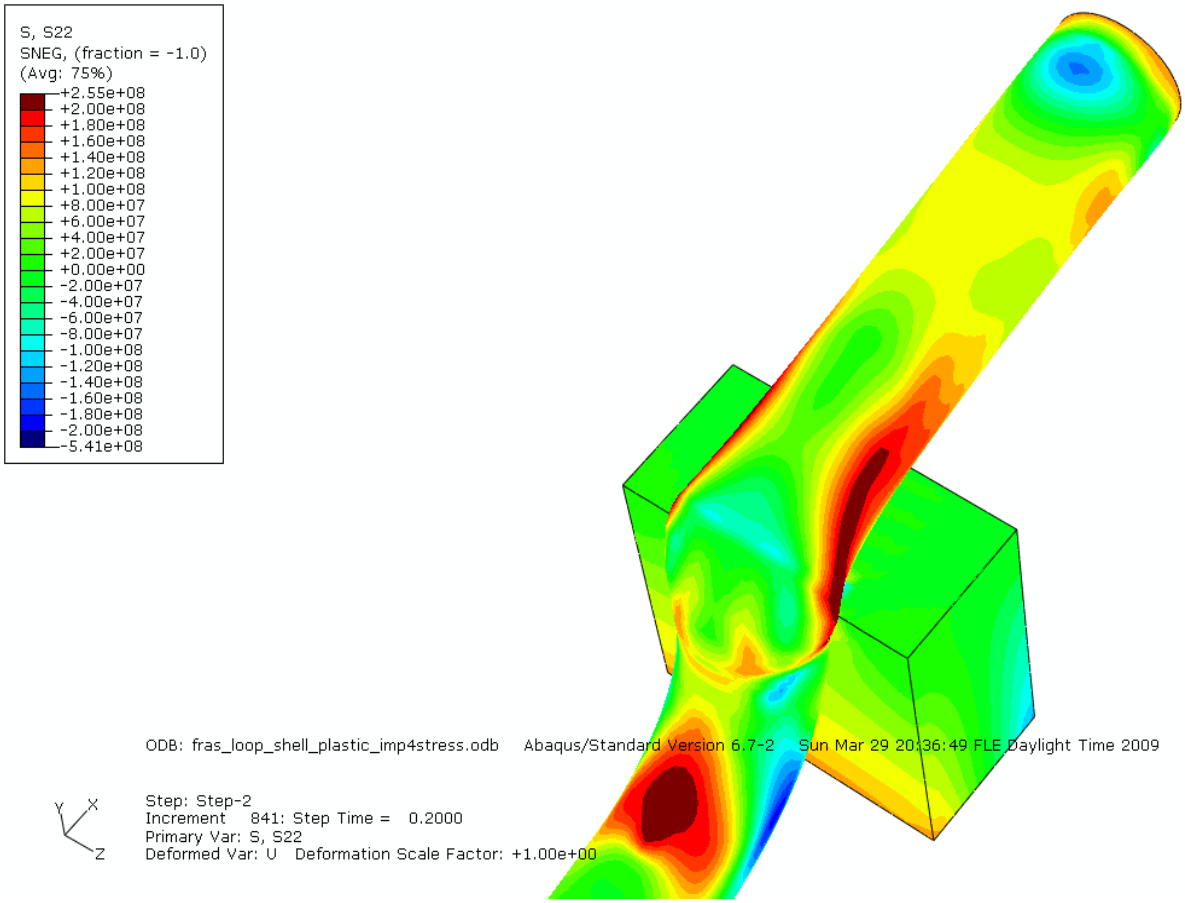

Figure 38. S22 [Pa] on the outer surface at 0.14 s and 0.20 s after the pipe break.

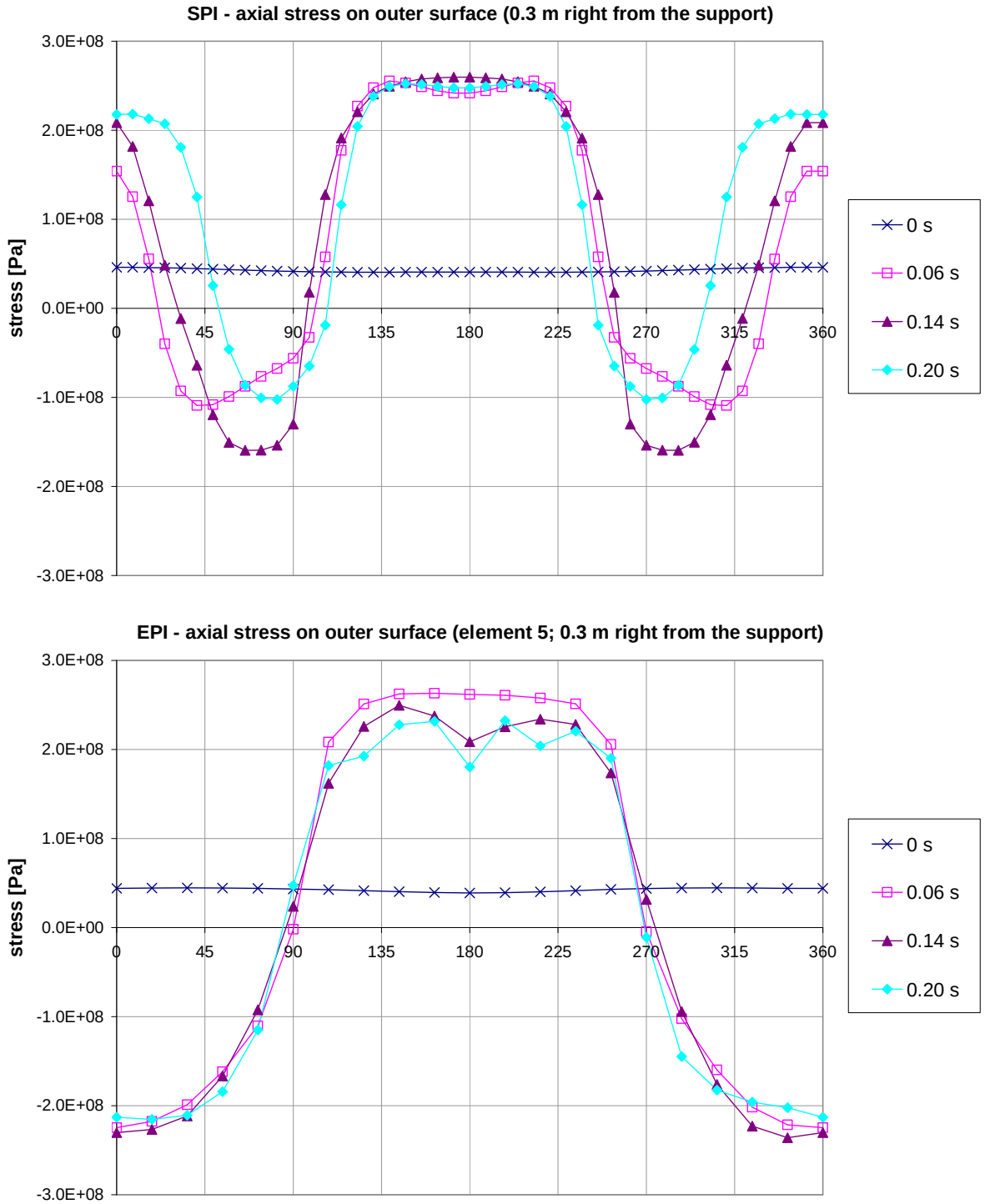

Figure 39. Axial stress [Pa] on the outer surface around the cross-section 0.3 m right from the support (cases SPI and EPI).

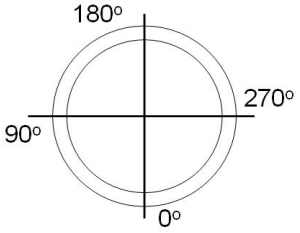

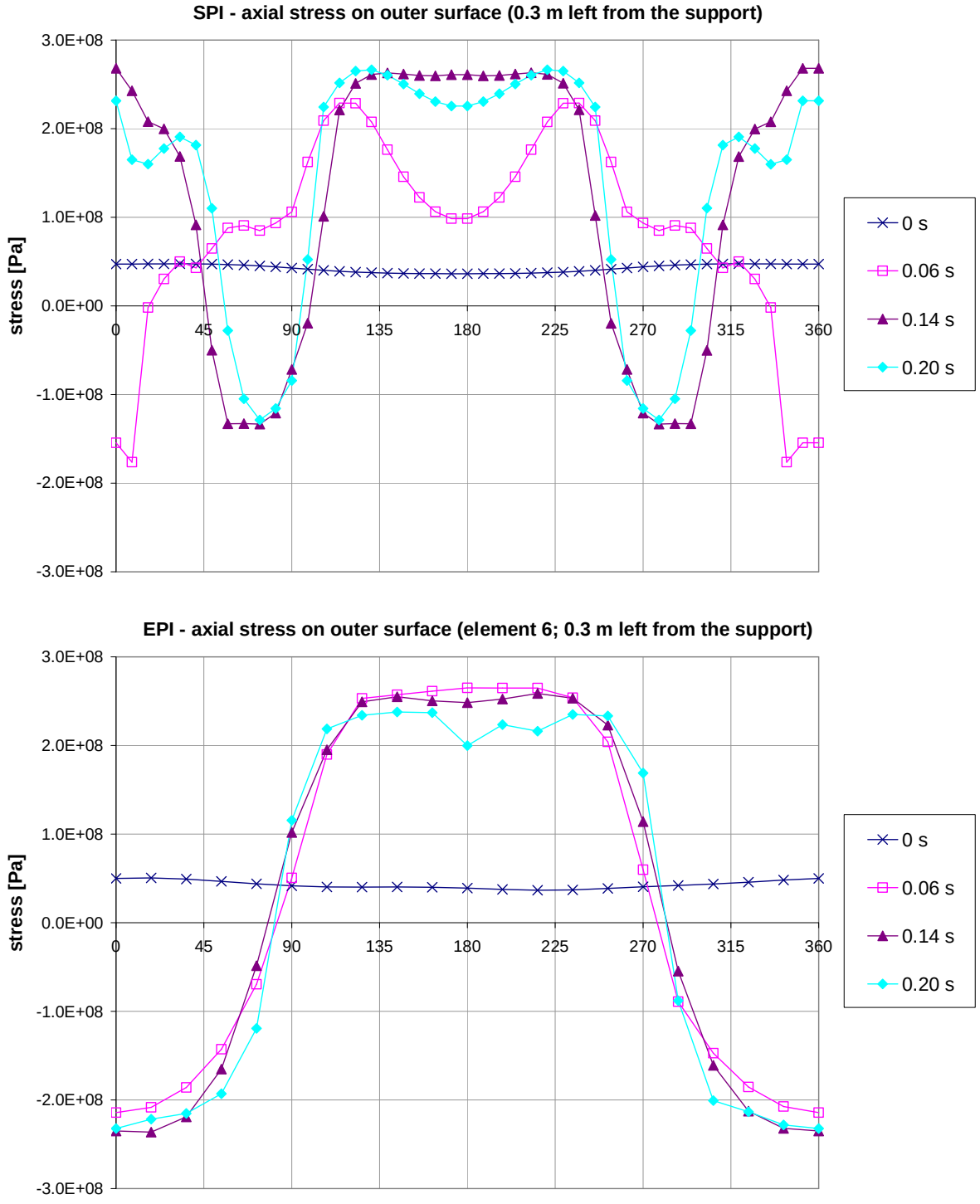

Figure 40. Axial stress [Pa] on the outer surface around the cross-section 0.3 m left from the support (cases SPI and EPI).

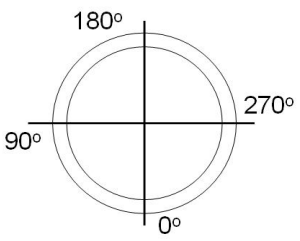

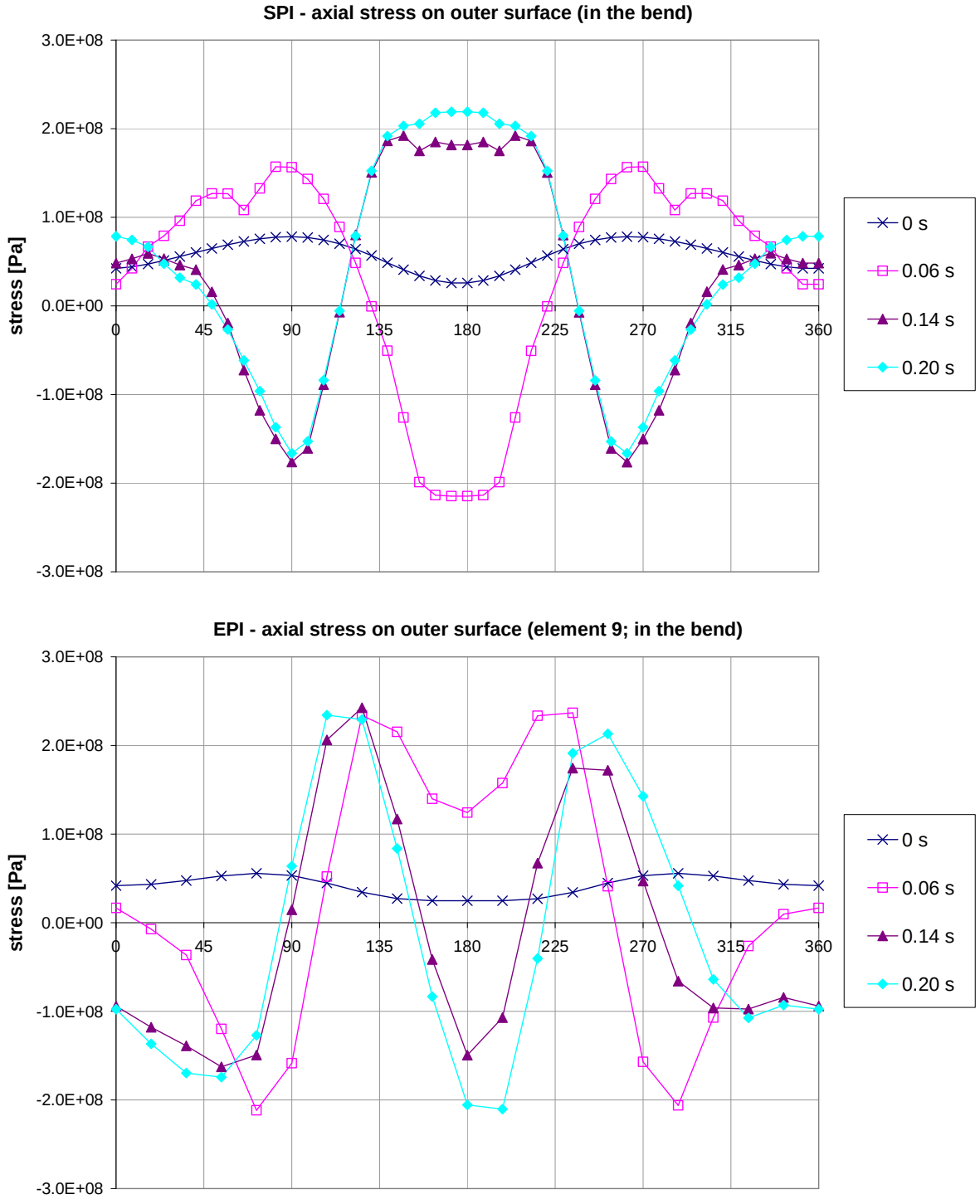

Figure 41. Axial stress [Pa] on the outer surface around the cross-section near the middle of the bend (cases SPI and EPI).

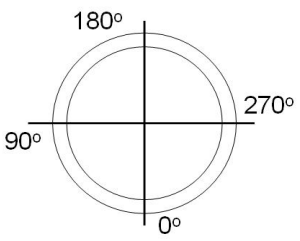

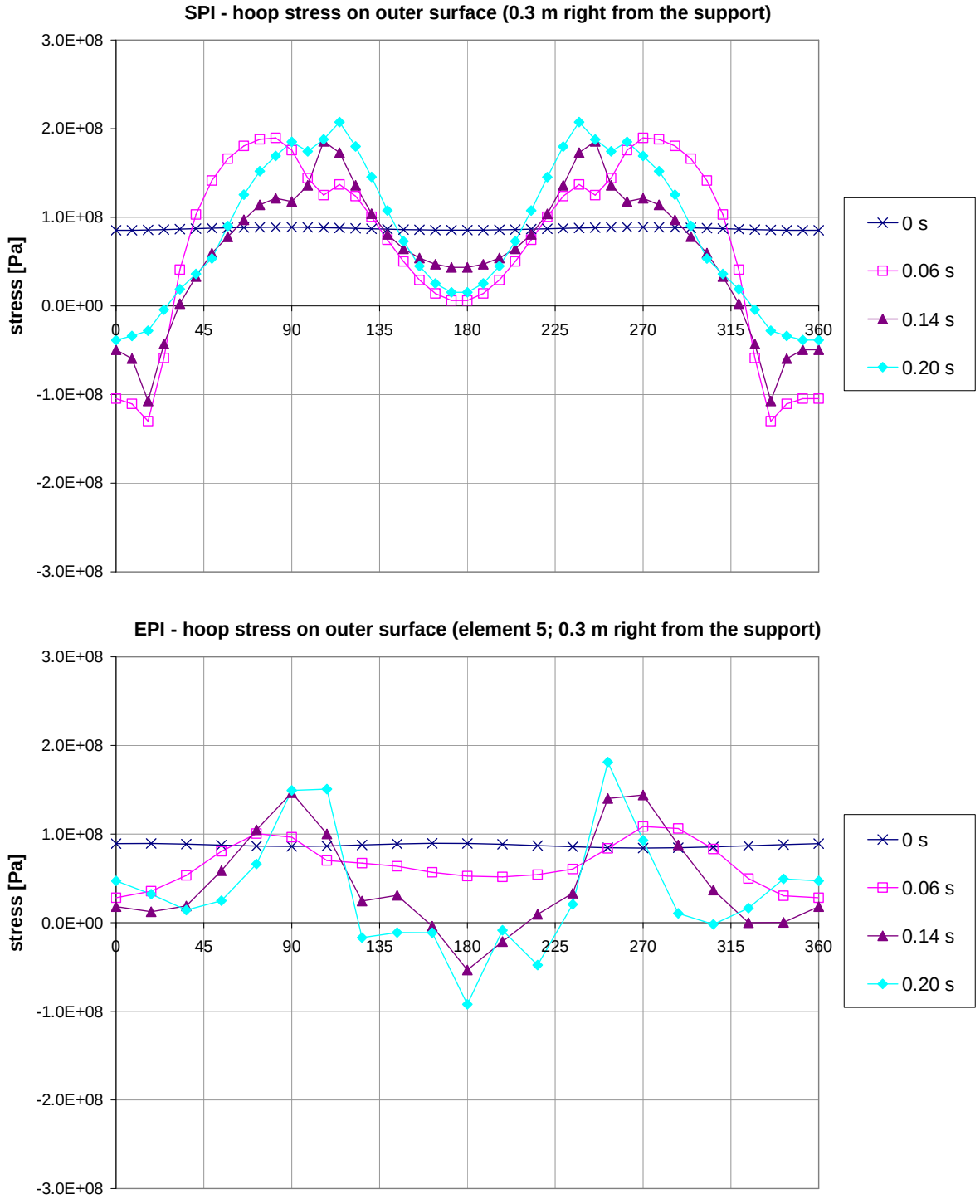

Figure 42. Hoop stress [Pa] on the outer surface around the cross-section 0.3 m right from the support (cases SPI and EPI).

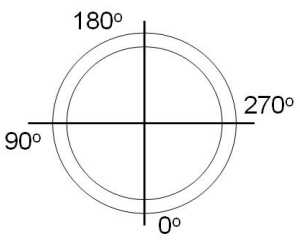

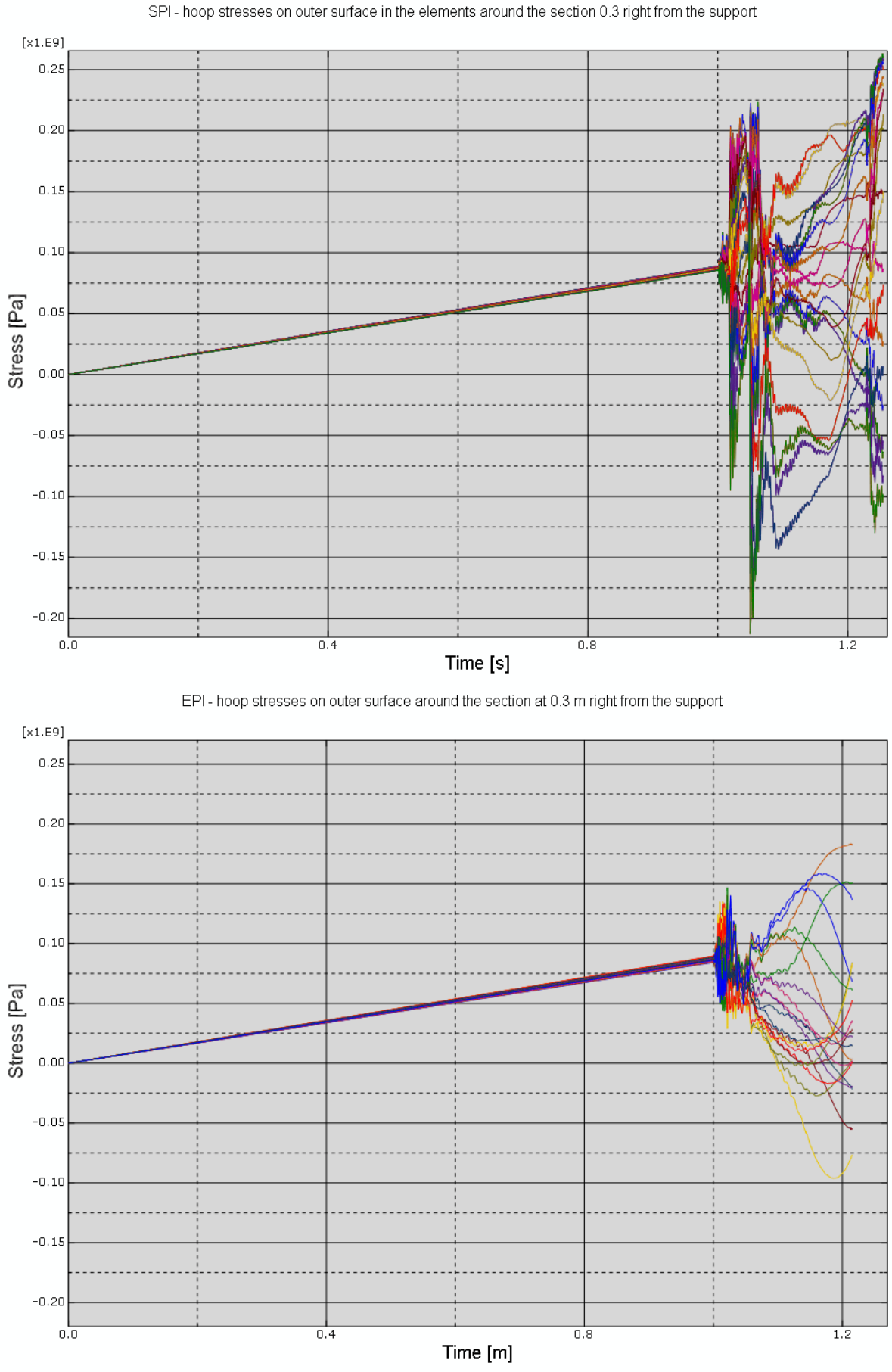

Figure 43. Hoop stresses [Pa] on the outer surface around the section 0.3 m right from the support as functions of time (cases SPI and EPI).

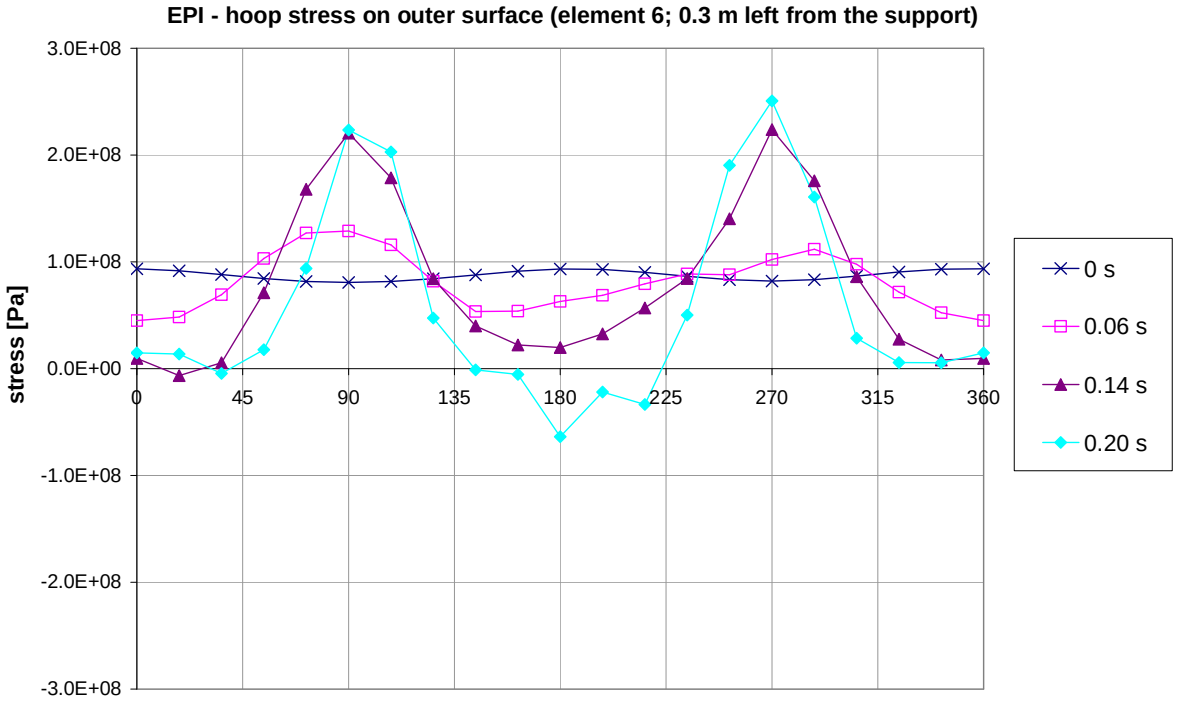

Figure 44. Hoop stress on the outer surface around the cross-section 0.3 m left from the support (case EPI).

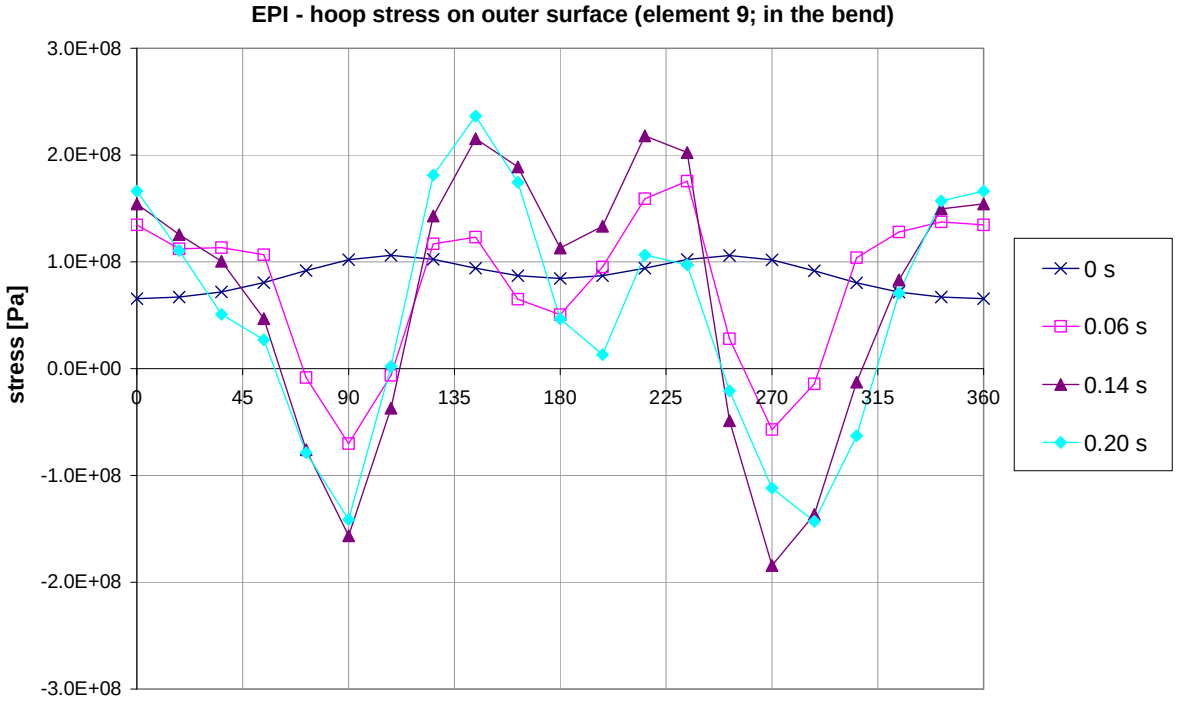

Figure 45. Hoop stress [Pa] on the outer surface around the cross-section near the middle of the bend (case EPI).

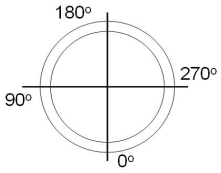

Figure 46 shows the shell element numbers on the side of the pipe near the support and the two element sets on the left and right side of the support (in red frame colour). Figure 47 shows the axial stresses in cases SPI and EPI in the corresponding location through the thickness of the wall at three different time instants; 0 s, 0.01 s and 0.04 s after the pipe break. The location is the element number 6743 in Figure 46 and the corresponding integration number in the section of element 6 in case EPI. In the x-axis, 1 stands for the inner surface and 5 stands for the outer surface of the pipe wall (see the integration points through the wall thickness in Figure 33). Before the pipe break, the axial stresses are in quite good correlation with each other in the two models, but right after 0.01 seconds, the stress distribution develops differently through the wall. After 0.04 seconds, the stress distributions correspond to each other quite well again.

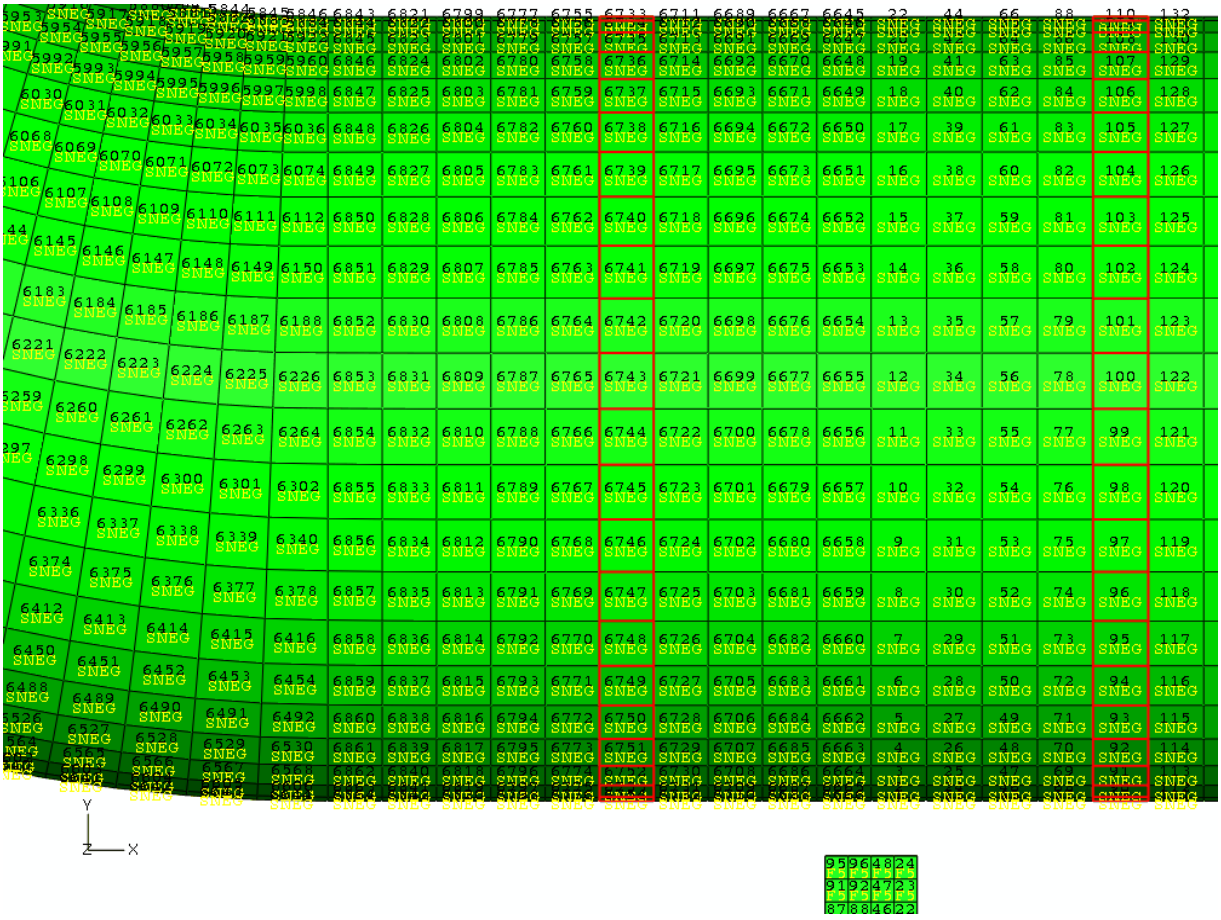

Figure 46. Shell element numbers on the side of the pipe near the support. Element number 6743 is used for the comparison with elbow element model.

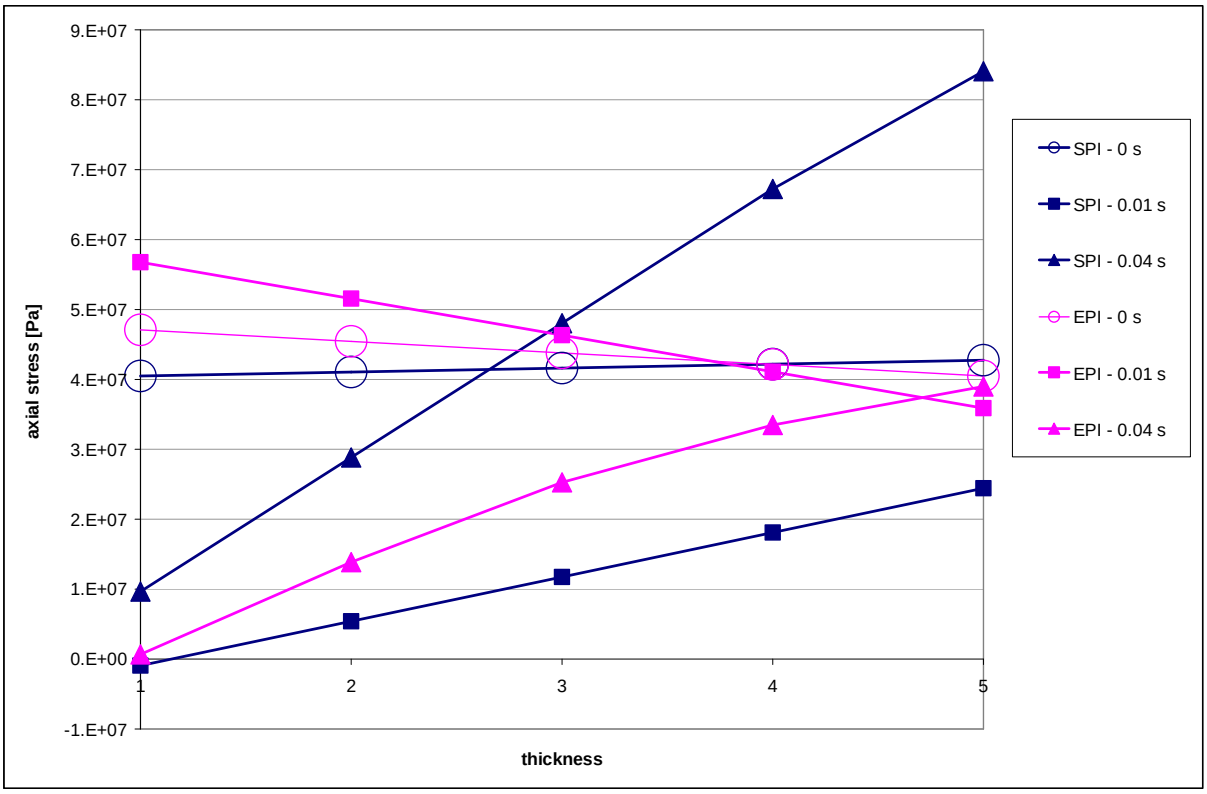

Figure 47. Axial stresses [Pa] in cases SPI and EPI in the corresponding location (shell element 6743) through the thickness of the wall at three different time instants.

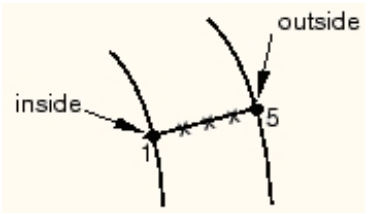

6 Conclusions and Future Work

In this paper, different kinds of ways to numerically model with finite element code Abaqus the power plant pipe runs and their supports are studied. A pipe guillotine break with whipping is chosen as a dynamic analysis case. Simple and typical pipeline geometry and materials are chosen. The test pipe line is modelled with different ways and the eigenfrequencies are compared with each other. The hydrodynamics of water or its mass are not included.

It is seen that in respect to the eigenmodes, the pipe element model is adequate and almost as accurate as a shell element model with a fine mesh, especially when the pipe bend is modelled with elbow elements. The stiffness of different components and the gap in a pipe impact to a restraint are evaluated and modelled with pipe or elbow and special-purpose elements. This is crucial when the restraints have to be simplified in extensive models with long pipe runs and many supports. The chosen restraint type is relatively stiff when having elastic material properties.

Finally, dynamic analyses of a pipe break are conducted with different models that are confirmed as adequate. A shell element model with a relatively dense mesh and an elbow element model are chosen to be compared. Both linearly elastic and nearly ideal plastic material properties are assigned to the steel of pipe and restraint. The calculated forces and stresses correspond to theory and the ones found in literature. The dynamic model behaviour also corresponds to the static model behaviour and the eigenmodes that are solved beforehand. In general level, the models behave in a similar manner. The plastic hinges develop at the same time and the pipe deforms globally in the same way.

Nonlinear spring elements are found to act realistically and seem very suitable to model restraints for this kind of dynamic problem. The displacement and cross-section deformation results of the elbow element model corresponded reasonably well to the ones of the much larger shell element model. The situation is naturally different on a detail level near the restraint. There are some local discrepancies in the stress results.

It should be remembered that comparisons were made between several FE models instead of an actual structure and FE models.

This is not an extensive study but gives a good base for the future study and for making the decision how to solve similar kinds of problems. All the different ways and combinations to model these cases were not studied, but a few adequate ways were found. Long pipe runs with many supports and restraints should preferably be modelled with simple structural elements such as pipe and elbow elements and special-purpose elements in order to save time and numerical errors due to overly large models. It is shown, how the stress distribution along the pipe axis, around the cross-section and through the thickness of the wall can be solved with elbow elements on a fairly detailed level.

A suggestion is to use for normal global vibration analyses approximately six ELBOW31 elements for the bends and PIPE31 elements of the same length for the straight parts. The same type of model with additional nonlinear spring elements is also adequate for simulations of pipe breaks.

Some future study suggestions can be made. The rate dependency of materials should be included. The plastic properties should be defined more carefully and they should correspond better the real nuclear power plant materials. The realistic model is found somewehere between the two material models chosen in this study.

Also, different types of supports and especially more spring-like and softer supports should be studied instead of the very rigid one considered here. The support structure was too complicated to be modelled with only a single spring element, if the nonlinear dynamic behaviour and the effects of the surrounding civil structures are to be taken into account. The spring elements are adequate when a longer section of a pipe line is examined and no extensive displacements and plastic hinges are anticipated. Especially the “tube support elements” are worth studying more in the future.

In case of pipe or elbow elements, the pipe break load should also be modelled with point loads that have certain predetermined amplitude. A denser mesh would give more detailed local stress results.

The utility routine felbow.f was not successfully deployed. It should create a data file that can be used in Abaqus/CAE to plot the current coordinates of the integration points around the circumference of the elbow section of interest and also other results around the section and along the length of the elbow element. Isoparametric contour plots should not be impossible with the help of felbow.f, other Fortran routines of the same kind and some commercial programmes such as Matlab.

At least the mass of water should be included. The sudden rapid decrease of the inner pressure after the pipe break should be taken into account. That can be done fairly easy by assigning different pressure amplitudes to different sections of the pipe. To be more accurate, hydrodynamic effects of water in a more detailed manner should be taken into account. That would require computational fluid dynamics and even bidirectional fluid-structure interaction.

More extensive pipeline geometry with different types of supports and restraints should also be studied.

References

Abaqus Manuals, 2007. Version 6.7-2. Abaqus inc.

Calonius, K., 2008. “Preliminary Numerical Studies on Dynamic Behaviour of Pipelines”. VTT Public Research Report, VTT-R-01637-08.

Haapaniemi, H., 2002. “Evaluation of Different Pipe Bend Modelling Schemes with Abaqus ELBOW31 Elements”. VTT Public Research Report, BVAL64-021212.

Micheli, I., Zanaboni, P. Transactions of the SMiRT Conference, 2003. Paper #J05-4. “An Analytical Validation of Simplified Methods for the Assessment of Pipe Whip characteristics”.

Vörös, G., Zsidi, Z., 2002. “Analysis of the effects of postulated pipe rapture”. Gépészet 2002, Budapest. 307-310.